# Performance Evaluation of PM, $NO_x$, and Hydrocarbon Removal in Diesel Engine Exhaust by Surface Discharge-Induced Plasma

Kohei Kawakami*, Ken Watatani**, Haruhiko Yamasaki*, **,

Tomoyuki Kuroki*, **, Masaaki Okubo*, **[*]

** Department of Mechanical Engineering, Osaka Metropolitan University, 1-1 Gakuen-cho, Naka-ku, Sakai 599-8531, Japan*

***Department of Mechanical Engineering, Osaka Prefecture University, 1-1 Gakuen-cho, Naka-ku, Sakai 599-8531, Japan*

*The final publication of this paper is

Kohei Kawakami, Ken Watatani, Haruhiko Yamasaki, Tomoyuki Kuroki, Masaaki Okubo, Performance evaluation of PM, NOx, and hydrocarbon removal in diesel engine exhaust by surface discharge-induced plasma, Journal of Hazardous Materials, Volume 462, 2024, 132685, https://doi.org/10.1016/j.jhazmat.2023.132685.

(https://www.sciencedirect.com/science/article/pii/S0304389423019684)

*Corresponding author: M. Okubo, Department of Mechanical Engineering, Osaka Metropolitan University, 1-1 Gakuen-cho, Naka-ku, Sakai 599-8531, Japan
Tel.: +81 72 254 9230; Fax: +81 72 254 9230.
*E-mail address*: mokubo@mokubo.com

**Abstract**

Diesel engines are characterized by low $CO_2$ emissions and high fuel efficiency. However, their exhausts contain nitrogen oxides ($NO_x$), particulate matter (PM), and hydrocarbons (HC) that require removal by aftertreatment. A novel low-temperature plasma-based aftertreatment method has been developed for the simultaneous removal of $NO_x$, PM, and HC. $NO_x$ could be reduced by reacting with HC and CO in the exhaust gas. The particle and gas concentrations in the exhaust are measured using a scanning mobility particle sizer, a $NO_x$ analyzer, and a total hydrocarbon analyzer. The treatment performance is evaluated using the resulting measurements. The diesel engine is operated under 0, 25, 50, and 75% loads (maximum output of 2 kW), and the exhaust gas is mixed with $N_2$ + $O_2$ (13%) gas. The power is adjusted to provide 100, 200, 300, and 400 W input power during the plasma reactor treatment. The aftertreatment removal of $NO_x$, PM, and HC is evaluated, and the engine exhibits a removal efficiency of 70% for $NO_x$, 98% for PM, and 67% for HC at 75% engine load and an input power of 100 W.

Keywords: Diesel engine, Surface discharge plasma, $NO_x$, PM, Hydrocarbon

## 1. Introduction

Diesel engines have long been favored in several segments of the vehicle industry. One of the core reasons for their popularity is their inherent capability to produce lower $CO_2$ emissions compared to their gasoline counterparts. Another compelling feature of diesel engines is their superior fuel efficiency, allowing them to move longer distances on a single fuel tank. These advantages make diesel engines a sustainable choice for long-haul transport and heavy-duty vehicles. Although every technology has its challenges, a significant concern is the exhaust gas for diesel engines. The exhaust from these engines consists of a mix of nitrogen oxides ($NO_x$), particulate matter (PM), and hydrocarbons (HC). These components, especially $NO_x$ and PM, are harmful to both the environment and human health. To curb these emissions, the introduction of aftertreatment technologies becomes indispensable [1–15]. The industry has relied on a few established aftertreatment methods. One of the most commonly employed is the selective catalytic reduction (SCR). Several studies on SCR [13–15] should be explained. The article [13] predicted the efficiency of the SCR system through modeling. The article [14] analyzed the treatment of $NO_x$, HC, CO, and other pollutants in the SCR system in detail through experiments. The article [15] identified the issue of urea crystallization in the SCR system. SCR works efficiently in reducing $NO_x$ emissions. However, it is not without its challenges. For SCR to function effectively, a urea water solution is needed, necessitating a separate storage tank. Over time, the SCR catalyst

degrades and must be replaced periodically. Another limitation is the inability of HC and $NO_x$ trap catalysts to be used with heavy oils, limiting their application in certain conditions.

Beyond the challenge posed by $NO_x$, the removal of particulate matter (PM), such as $PM_{2.5}$, is a significant concern, particularly in the East Asian region. Upon inhalation, it gets lodged in the lungs and detrimentally impacts human well-being. Consequently, there has been global attention directed towards its mitigation. Indoor air cleaners containing electrostatic precipitators and high-efficiency particulate air (HEPA) filters prove efficacious in eliminating airborne PM. Employing these air purifiers indoors can lead to a substantial reduction in PM levels [2, 3]. Diesel particulate filters (DPF) have emerged as a leading solution in this domain. These filters are integrated into most modern diesel automobiles, ensuring they meet stringent annual emissions regulations [16–18]. However, again, DPFs are not free from complications. As they trap particulates, they need regular maintenance. Over time, PM accumulates, leading to a high-pressure drop and clogging of the filter. Thus, passive regeneration, which is done continuously, and active regeneration, which is periodic high-temperature burn-off, are essential to maintain the DPF's efficiency [19–25]. The passive regeneration is made with catalysts while active regeneration is made with electric heaters or afterburners.

In the development of the automobile industry, hybrid-powered vehicles, which combine the power of traditional combustion engines and electric motors, are gaining traction. With

this evolution, there is a significant shift in aftertreatment technologies, too.

Low-temperature plasma, an innovation harnessing electrical energy, stands out as a promising technology. Unlike traditional methods, it does not rely on ammonia or catalysts for $NO_x$, PM, and HC removal [26–45]. Low-temperature plasma, in essence, leverages high voltage to generate a plasma field. Within this field, reactive oxygen species, known for their strong oxidizing power, are produced. These species then interact with $NO_x$, PM, and HC, effectively breaking them down. The advantages are manifold. For instance, this technology can treat low-temperature exhaust gases continuously. Additionally, it does not experience the same pressure drop issues as DPFs, making it a viable alternative [42]. Some papers will introduce research on the treatment of hydrocarbons and $NO_x$. The paper [43] investigates the use of a plasma/adsorbent system to treat $NO_x$ emissions in diesel exhaust. By using solid industrial wastes as the adsorbent, the authors present a potentially sustainable method for $NO_x$ reduction, simultaneously addressing pollution and waste management issues. The paper [44] evaluates the performance of waste foundry sand and bauxite residue in reducing $NO_x$ emissions from diesel exhaust. The paper [45] introduces a novel system, employing cascaded plasma-ozone injections, to decrease total hydrocarbon emissions from diesel exhaust. The results were promising and activating inexpensive adsorbents and catalysts with plasma opens the way to various industrial applications for environmental cleaning.

In a previous study [46], a plasma reactor and high-frequency, high-voltage power supply,

92 which were the components of a plasma aftertreatment system, were installed to conduct new
93 tests with the aim of applying it practically as a PM aftertreatment technology to meet future
94 emission regulations. Evidently, PM oxidation removal by surface discharge plasma was
95 confirmed, thus indicating the possibility of the simultaneous removal of PM and $NO_x$ [27,
96 28, 46, 47].
97 In this study, we treat a plasma filtration technique aimed at extracting particulate matter
98 (PM) while it is airborne, achieved by directly subjecting PM-laden gas to plasma. Within
99 this approach, PM gets eliminated through chemical reactions and the particle-collecting
100 influences inherent to plasma. This is realized by guiding PM-containing gas through a
101 cylindrical plasma reactor housing surface discharge electrodes. Because minimal pressure is
102 lost and performance degradation over extended operation periods is negligible, the process
103 remains efficient and uninterrupted, obviating the need for filter rejuvenation or cleansing.
104 Additionally, the reactor exhibits the capability to eliminate nitrogen oxides ($NO_x$ = NO +
105 $NO_2$), odors, and gases containing volatile organic compounds (VOCs). The primary aim of
106 this current investigation is to explore a plasma system capable of accommodating
107 substantial filtration volumes, enhancing the enduring presence of radicals, and amplifying
108 the overall decomposition efficiency of the system. Furthermore, to evaluate the treatment
109 performance, the particle and gas concentrations (NO, $NO_x$, CO, $CO_2$, $O_2$, HC, $HNO_3$, and
110 $O_3$) are measured. Additionally, to compare reactor performance at these loads, experiments

are conducted with engine loads of 0, 25, 50, and 75 %. In summary, as the vehicle industry progresses, the imperative to find efficient, cost-effective, and sustainable aftertreatment solutions grows. While traditional methods like SCR and DPF have their place, innovations like low-temperature plasma offer a glimpse into a cleaner future for diesel engines.

## 2. Experimental setup and methods

### 2.1 Experimental setup

**Fig. 1(a)** shows a schematic of the experimental setup for the diesel engine exhaust treatment system using a surface discharge plasma reactor. The experimental apparatus consists of a diesel engine (KDE2.0E, Wuxi Kipor Power Co., Ltd.) exhaust flow path and dilution cylinder flow path, which are mixed and diluted before entering the plasma reactor to treat the $NO_x$, PM, and HC in the exhaust gas. In the figure, $N_2$ cylinder gas (secondary pressure fixed at 0.2 MPa) and synthetic air cylinder gas ($N_2$ = 79 %, $O_2$ = 21 %, secondary pressure fixed at 0.2 MPa) are used as the dilution gases. The $N_2$ cylinder gas and synthetic air are mixed at an $O_2$ concentration and flow rate of 13 % and 2.5 L/min, respectively, using a set of mass flow controllers (SFC280, Hitachi Metals, Ltd.), with maximum flow rates of 5 and 10 NL/min (N indicates the standard state of 0 °C, one pressure). Additionally, flow meter A (RK1710, KOFLOC Corp.; maximum flow rate = 5 NL/min) is used to adjust the flow rate of the dilution gas. Further, to evaluate the removal performance of $NO_x$, PM, and

HC, the exhaust gas passes through a plasma reactor. Thus, the $O_2$ concentration in the reactor must be matched with that of the exhaust gas. Therefore, dilution gas with an $O_2$ concentration of 13 % is prepared as the $O_2$ concentration of diesel engine exhaust gas is approximately 13 %. In this experiment, the diluted gas (flow rate = 2.5 L/min) is mixed with the exhaust gas, and the mixed gas (flow rate = 5 L/min; dilution ratio = 2.0) is prepared and tested. The reason for dilution is that if the exhaust gas is used without dilution, the PFA tube becomes clogged, and particles become trapped because of the effects of the large amount of soot contained in the exhaust gas and water vapor in the exhaust gas adhering to the PFA tube in the flow path, thus rendering difficulty in obtaining accurate experimental data and conducting the experiment. It is noted that $O_2$ concentration of the raw exhaust gas is almost the same as the diluted gas. Therefore, the dilution has little effect on the reaction pathways of the plasma reactor. The mixed gas is pressurized using a pump (APN-110LVX1-2, Iwaki Co., Ltd.; maximum discharge pressure = 0.10 MPa), and the flow rate is adjusted to 5 L/min using a flow meter C (RK1710, KOFLOC Corp.; maximum flow rate = 5 L/min). Next, the gas mixture is introduced into the plasma reactor, where PM and HC are oxidized and removed by the surface discharge plasma. The concentrations of $HNO_3$ and $O_3$ in the exhaust gas after the treatment are measured using gas detector tubes (No. 15L nitric acid, No. 18M ozone, GASTEC CORPORATION) through a gas detector tube sampling port. Note that the treated exhaust gas contains the $O_3$ generated in the reactor, which may corrode and damage

149 the measurement equipment. Therefore, a tubular furnace (KPO-14K, Isuzu Seisakusho Co.,
150 Ltd.) is installed immediately after the reactor to perform pyrolysis at a set temperature of
151 300 °C. Three-way valves A and B are installed to prevent the exhaust gas from flowing into
152 the reactor by changing the flow path when the reactor is turned off. When the exhaust gas
153 flow into the reactor, water vapor and particles accumulate and negatively affects the
154 measurement.

155 After treatment in the plasma reactor, the gas is divided into two flow paths. The exhaust
156 gas is adjusted to a flow rate of 4.0 L/min using flow meter E (RK1710, KOFLOC Corp.;
157 maximum flow rate = 5 L/min), and particles are removed using an air filter (ZFC-EL-4,
158 SMC Corporation) and hollow fiber membrane filter (DRY7-1/4, KITZ Corporation).
159 Subsequently, a set of gas analyzers (PG-235 and PG-240, HORIBA, Ltd.) and total
160 hydrocarbon (THC) or total volatile organic fraction (TVOC) analyzer (FV-250, HORIBA,
161 Ltd.) are used to measure the gas components (NO, $NO_x$, $O_2$, CO, and $CO_2$) and THC,
162 respectively. In the other flow path, the flow rate is adjusted to 1 L/min, and the gas is
163 sampled using flow meter D (RK1650, KOFLOC Corp.; maximum flow rate = 1 L/min). The
164 sampled gas is diluted to 1/5 concentration with $N_2$ cylinder gas (secondary pressure fixed at
165 0.1 MPa) using flow meter B (RK1710, KOFLOC Corp.; maximum flow rate = 5 L/min) and
166 measured using a scanning mobility particle sizer (SMPS). The SMPS is comprised of a
167 differential mobility analyzer (DMA, Model 3080, measurement range of particle size: 10 to

414 nm, TSI Inc.) and a condensation particle counter (CPC, Model 3787, TSI Inc.). As the particle concentration $dN/d\log D_p$ in the CPC measurement ranges from 0 to $2.5 \times 10^5$ ($cm^{-3}$), dilution with $N_2$ gas is necessary to avoid exceeding the upper limit of $2.5 \times 10^5$ ($cm^{-3}$). Additionally, the current, voltage, and power waveforms in the reactor are measured using an oscilloscope (DLM3054, Yokogawa Electric Corporation) using a current probe (MODEL 2878, Pearson Electronics, Inc.; 10 A/V) and a high-voltage probe (HV-P60, Iwatsu Electric Co., Ltd.; 2 kV/V). The exhaust gas and reactor surface temperatures are measured using thermocouple thermometers (MTCTS, MISUMI Group Inc. and AD-5602, A&D Company, Limited, respectively).

**Fig. 1(b)** shows a photograph of the diesel engine, exhaust piping, apparatus, and flow directions used in this experiment. The diesel engine exhaust gas obtained from the sampling port has a high temperature and contains water vapor, which is removed and cooled by passing it through a drain pot.

## 2.2 Plasma treatment system

### 2.2.1 Overview of plasma reactor equipment

**Fig. 2** shows the cylindrical surface discharge element (HCII-OC70, Masuda Research Inc.) constituting the surface discharge plasma reactor used in this experiment. **Fig. 2(a)** shows a schematic of the cylindrical surface discharge element and cross-section of the inner

187 wall of the element. The exhaust gas flows in through the sample inlet and flows out through
188 the sample outlet after being treated with plasma. The equipment consists of a surface
189 discharge tube utilizing the surface discharge induced plasma chemical process (SPCP
190 discharge tube: OC-70/AC, Masuda Research Inc.) technology and a high-frequency and
191 high-voltage power supply (HCII-70/2, input: voltage = three-phases 200 Vac, power = 1.5
192 kVA (50/60 Hz), output: peak-to-peak voltage = 14 kV (no electrical load), input power =
193 70−860 W, frequency = 9.9 kHz, Masuda Research Inc.). **Fig. 2(b)** shows the front view of
194 the surface discharge element and the high-frequency and high-voltage power supply. The
195 element is a ceramic tube (outer diameter = 80 mm; length = 300 mm) with a discharge
196 electrode on its surface of the ceramic tube and an induction electrode inside the ceramic. A
197 surface discharge is extended along the inner walls of the discharge electrode and ceramic
198 tube by applying a high frequency and voltage between the two electrodes. Thus, a surface
199 discharge plasma is generated on the surface of the discharge electrode, thereby producing
200 reactive free radicals (active oxygen (O) and nitrogen (N)) with strong oxidation properties.
201 The PM, HC, and $NO_x$ in the exhaust gas react with these active oxygen species for their
202 removal. Air cooling of the heat-dissipating fins attached to the outer wall of the ceramic
203 tube prevents overheating of the surface discharge elements. **Figs. 2(c)** and **2(d)** show the
204 internal structure of the reactor, as photographed by the endoscope. **Fig. 2(c)** shows the
205 results when the power is turned off, whereas **Fig. 2(d)** shows the results when the reactor

input power is 400 W. These images show that the discharge is generated along the electrodes on the ceramic surface.

### 2.2.2 Experimental condition and measurement procedure

**Table 1** shows the engine specifications and experimental conditions. **Fig. 3** shows the relationship between each composition of the raw exhaust gas components and the engine load. Regarding $CO_2$, NO, and $NO_x$, the values increase as the load increases. Regarding THC, $O_2$, and CO, the values decrease with increasing load. This graph gives the exhaust boundary conditions of the experiments. The input power to the plasma power supply is set to 0, 100, 200, 300, and 400 W, and the particle-removal efficiency of the reactor, discharge power, and concentration changes in the engine exhaust are measured. The time required for each power level to stabilize is 10 min. To determine the particle concentration before removal, the particle concentration is measured using the SMPS when the reactor is turned off. Subsequently, the flow path is changed using three-way valves A and B, and the reactor is turned on and allowed to stabilize for 10 min. After stabilization, measurements are taken using the SMPS and an oscilloscope, and these are used as the results when the reactor is turned on. The state of the reactor is alternately repeated three times between off and on conditions, and the measurements are performed under one condition. The gas concentration before the treatment is the average value of the 1-min period immediately before the reactor

is turned on. The gas concentration after the treatment is the average value at 1 min after the reactor power stabilized. During the measurement of one condition, changes in the exhaust gas components over time are recorded. In this experiment, the engine load is changed to 0, 25, 50, and 75 %, and the reactor removal performances at each engine load are compared. When the engine load is 100%, the exhaust gas concentrations fluctuates greatly because it is a critical condition of the engine performance. Therefore, the experiment could not be conducted because it was not possible to dilute the flue gas accurately, and to compare the gas concentrations before and after the treatment accurately. For all the conditions, the engine and gas analyzer warm-up times are both 60 min. Under each condition, the particle size distribution and gas concentration in the engine exhaust are measured using an SMPS, gas analyzer, and gas detector tube.

### 2.2.3 Reactions of PM, HC, and $NO_x$ in the plasma reactor

Diesel exhaust particles (DEP) contain dry soot (C), soluble organic compounds (SOF), hydrocarbon compounds (HC), sulfates, and water droplets. PM (C, SOF, and HC) is oxidized by active oxygen species, and gaseous CO and $CO_2$ are induced. Thus, PM may be treated spatially. The main chemical reactions for PM oxidation and removal are shown in reactions (1)–(11) [16, 25, 27, 28].

$O_3 \rightarrow O_2 + O$ (1)

$NO + O \rightarrow NO_2$ (2)

$NO_2 \rightarrow NO + O$ (3)

$C + 2O \rightarrow CO_2$ (4)

$C + O \rightarrow CO$ (5)

$CO_2 \rightarrow CO + O_2/2$ (6)

$SOF + O \rightarrow mCO_2\,(mCO) + nH_2O$ (7)

$2HC + 5O \rightarrow 2CO_2 + H_2O$ (8)

$2HC + 5NO \rightarrow 5N_2/2 + H_2O + 2CO_2$ (9)

$2NO_2 + 2C \rightarrow N_2 + 2CO_2$ (10)

$2NO_2 + 4C \rightarrow N_2 + 4CO$ (11)

(*m*, *n*: Integers)

In these reactions, according to reactions (4)–(8), C, SOF, and HC are oxidized by oxygen radicals induced by reactions (1)–(3). Simultaneous reduction of NO and HC is induced by reaction (9). Simultaneous reduction of $NO_2$ and dry soot is induced by reactions (10) and (11).

## 3. Results and discussion

### 3.1 Particle concentration and removal efficiency

**Fig. 4** shows particle concentration before and after plasma treatment for engine loads of: (a) 0%, (b) 25%, (c) 50%, and (d) 75 %. The particle size distribution of PM in the mixed gas is measured to confirm the PM treatment performance of the reactor for each engine load (sampling flow rate, $Q$ = 5 L/min, and dilution air flow rate, $Q_A$= 2.5 L/min). The horizontal and vertical axes represent the particle diameter (nm) and particle concentration of $dN/d\log D_p$ ($cm^{-3}$), respectively. Each symbol indicates the particle concentrations before and after treatment at 100, 200, 300, and 400 W. Additionally, each symbol represents the average value of the measurements, and each error bar represents the standard deviation $\pm\sigma$. The figure shows that the reactor performs well in PM removal at each load and input power based on particle concentration measurements. As the load increased, the peak value of the particle diameter distribution before treatment transitioned to a larger particle diameter range. This is speculated to be due to the fact that the PM particle diameter is larger, and the percentage of coarse particles increases as the engine load increases. Generally, there is a tendency for the diameter of diesel engine exhaust particles to increase as the engine load becomes larger. When the engine load increases, the combustion process becomes more efficient, leading to an increase in particle generation, which could result in larger particle diameters. However, this can vary depending on specific conditions and engine design. The following papers [48–50] provide information about diesel engine exhaust particles. Each

paper focuses on the characteristics of particles under specific engine load conditions. PM is composed primarily of soot and the soluble organic fraction (SOF), which are carbon components. Organic components, such as SOF, attach to the surface of agglomerates formed by the aggregation of soot particles and are emitted as PM. As the engine load increases, soot particle agglomerates tend to form more soot particles, SOF, and agglomerates. In addition, the combustion temperature in the engine increases, and small particles are burned. Consequently, as the number of small particles decreases, the proportion of coarse particles increases. These observations suggest that the peak concentration of particles before treatment is likely to shift toward larger particle diameters.

**Fig. 5** shows particle removal efficiency for engine loads of: (a) 0%, (b) 25%, (c) 50%, and (d) 75 %. The horizontal and vertical axes represent the particle size (nm) and removal efficiency (%), respectively. The symbols indicate the removal efficiencies after treatment with input powers of 100, 200, 300, and 400 W. When the particle concentration before treatment at each particle diameter is less than 2 % of the peak value, it is excluded to ensure measurement accuracy. The figure shows that in the particle size range of 23.8 nm and above, the averaged removal efficiency is higher than 96 % for all loads and input powers except for a plot point protruded from the frame of **Fig. 5(c)**. The plot point is the removal efficiency of 95% and standard deviation of 3.35 for the particle size of 20.2 nm at the power of 200 W. However, it is found that for the particle size range of 10−40 nm, the nucleation mode

particle removal efficiency is relatively lower, as shown in **Fig. 5(c)**. This indicates that a surface discharge plasma reactor provides high performance for PM removal.

### 3.2 Gas concentration over time during engine load change

**Fig. 6** shows time-dependent gaseous concentrations (input power $P$ = 100 W) for various engine loads of: (a) 0%, (b) 25%, (c) 50%, and (d) 75 %. In the figure, the horizontal axis represents the elapsed time (s); the left vertical axis represents the concentrations of CO, $CO_2$/10, $O_2$/100 (ppm), and THC × 10 (ppmC); and the right vertical axis represents NO and $NO_x$ concentrations (ppm). It is noted that the THC unit of ppmC means methane ($CH_4$) equivalent concentration. The two-direction arrows indicate the periods in which the power is turned on (ON) and off (OFF). The dotted line indicates the time that the flow path is switched with the three-way valves A and B to measure the particle concentration, and the gas concentrations instantaneously change. To determine the particle concentration before removal, the particle concentration is measured during the period when the reactor is turned off. Subsequently, the reactor is turned on and maintained for 10 min to stabilize the power. After the stabilization, the particle diameter distribution, reactor discharge power, and $O_3$ and $HNO_3$ concentrations are measured. This process of turning on and off is repeated three times for each power level. It is noted that the reason why there is a difference between the first time and the second time is that the first time measurement was affected by the previous

experimental conditions. For example, although **Fig. 6(b)** is a measurement result at $P$ = 100 W, it is considered that it was affected by the post-treatment gas at 200 W that was performed previously. It is difficult to completely remove this effect due to experimental time constraints. Repeating these experiments more consistently will be considered in future work. The figure shows that the NO, $NO_x$, and THC concentrations decrease, whereas the CO concentration increases when the reactor is turned on. The HC is oxidized by the active oxygen species such as oxygen (•O) and hydroxyl (•OH) radicals generated by the discharge plasma [43–45, 47].

**Fig. 7** shows typical time-dependent gaseous concentrations with an engine load = 75 % and input power = 400 W. Evidently, the THC concentration decreases, whereas the NO, $NO_x$, and CO concentrations increase owing to the formation of NO and $NO_x$ by the active nitrogen generated in the reactor for large power of 400 W. When the plasma is turned off, $CO_2$ concentration is increasing. This could be mainly caused by $CO_2$ reduction to CO when the plasma is turned on. Under the conditions in **Fig. 7**, a carbon balance is achived before and after treatment within the range of measurement accuracy. A similar trend to that in **Fig. 7** is observed at loads of 0, 25, and 50 % loads (input power, 400 W).

### 3.3 Gaseous concentrations before and after treatment for various engine load

**Fig. 8** shows the gaseous concentrations before and after the treatment for various engine

loads, with input powers of: (a) 100 W, (b) 200 W, (c) 300 W, and (d) 400 W. The horizontal axis represents the load (%), the left vertical axis represents the concentrations of CO, $CO_2$/10 (ppm), and THC × 10 (ppmC), and the right vertical axis represents NO, $NO_x$, $HNO_3$, and $O_3$ (ppm). The solid lines indicate the gas concentration after treatment, and the dotted lines indicate the gas concentration before treatment. It is noted that the gas concentration values used in the comparison before and after treatment shown in **Fig. 8** are the average values for one minute immediately before turning on and off of the reactor. Since the value during that time was stable, the stabilization time of 10 min is reasonable.

**Fig. 8(a)** shows that the NO, $NO_x$, and THC concentrations after treatment decrease at an input power of 100 W for all engine loads. Essentially, the simultaneous removal of $NO_x$, PM, and HC is achieved. As $HNO_3$ is generated at this time, the reduced NO and $NO_x$ first react with active oxygen species such as ozone, oxygen, hydroxyl radicals etc., and then with water in the exhaust gas to generate $HNO_3$. The $O_3$ concentration decreases, whereas the $HNO_3$ concentration increases with increasing load. More than 57 % HC removal is achieved at all loads and powers. The highest removal efficiencies of 70, 98, and 67 % for $NO_x$, PM, and HC, respectively, are achieved at a 75 % engine load because the amount of water in the exhaust gas increase at higher loads, which enhances the conversion of $NO_x$ to $HNO_3$.

**Fig. 8(b)** shows that the NO and $NO_x$ concentrations increase after treatment at an input power = 200 W. The amount of $HNO_3$ generated is insignificant. Increased NO and $NO_x$

concentrations vary with the load owing to the influence of exhaust gas components. As the engine load increases, the $CO_2$ concentration increases, whereas the THC and CO concentrations before the treatment decrease. This is owing to an increase in the combustion temperature of the engine and the ratio of completely combusts PM to HC in the exhaust gas.

**Figs. 8(c)** and **(d)** show that the trends at input powers of 300 and 400 W are similar to that at 200 W. The results reveal that the system performs well at an input power of 100 W for $NO_x$, PM, and HC simultaneous removal. Combined with a wet scrubber for $HNO_3$ removal and a catalyst bed for $O_3$ removal followed by the plasma reactor, absorption, neutralization, and removal enable the simultaneous removal of $NO_x$, PM, HC, $HNO_3$, and $O_3$, and a total pollution control system will be realized. The trend with some hypothesis and reaction kinetics in the plasma discharge zone are discussed in the next section.

### 3.4 $NO_x$, PM, and HC removal for various specific energy

**Fig. 9** shows the results of $NO_x$, PM, and HC removal efficiencies for various specific energy. The horizontal and vertical axes represent the specific energy (*SE*) (J/L) and removal efficiency (%), respectively; the symbols indicate the removal efficiencies of $NO_x$, PM, and HC, respectively. The specific energy is calculated dividing the discharge power by the flow rate of 5 L/min = 0.0833 L/s. The PM removal efficiency is obtained from the values shown in **Fig. 5**. $NO_x$ and HC removal efficiencies are calculated from the $NO_x$ and HC

377 concentrations before and after treatment, as shown in **Fig. 8**. Note that a $NO_x$ removal of
378 less than zero is excluded. Therefore, $NO_x$ plots are fewer $NO_x$ plots than those for PM and
379 HC. At an input power of 100 W or *SE* less than 824 J/L, $NO_x$ in the exhaust gas is reduced
380 and removed by reacting with HC and CO in the exhaust gas through the following reactions.
381
382 $$2NO + 2CO \rightarrow N_2 + 2CO_2 \quad (12)$$
383 $$2NO_2 + 2CO \rightarrow N_2 + O_2 + 2CO_2 \quad (13)$$
384 $$4NO + 2HC \rightarrow 2N_2 + 2CO_2 + H_2 \quad (14)$$
385 $$4NO_2 + 2HC \rightarrow 2N_2 + 2CO_2 + H_2 + 2O_2 \quad (15)$$
386
387 It is known from the figure that more than 98 % removal of PM, 70 % removal of $NO_x$, and
388 67 % removal of HC are achieved at a specific energy of 634 J/L. Concerning about HC
389 removal, removal efficiency is almost constant irrespective of *SE* because the exhaust gas
390 contains a certain concentration of hydrocarbons which are difficult to be decomposed by the
391 plasma, such as monocyclic and polycyclic aromatic hydrocarbons. The decomposition
392 efficiency of each component of the hydrocarbon have not been measured, and it should be
393 done in future research. At a power of 200 W or more, the exhaust gas reaches a temperature
394 of about 80 °C, and the plasma produces $NO_x$ at a concentration higher than the $NO_x$ can be
395 reduced by HC and CO. Therefore, $NO_x$ removal efficiency becomes negative. This suggests

396 that this exhaust gas treatment system can achieve a high treatment performance when
397 operated at low specific energy.
398
399 **4. Conclusions**
400 A performance evaluation of PM, $NO_x$, and HC removal from diesel engine exhaust by
401 surface-discharge-induced plasma is performed. The main conclusions are as follows.
402 (1) At 100 W input power, $NO_x$, PM, and HC are removed at engine loads, with top
403 efficiencies of 70% for $NO_x$, 98% for PM, and 67% for HC at 75% load. $NO_x$ reduces
404 by interacting with HC and CO. Increasing CO concentration leads to PM and HC
405 oxidation from reactive oxygen species such as O in plasma discharge. Furthermore,
406 simultaneous reduction of NO and HC, and simultaneous reduction of $NO_2$ and dry soot
407 are induced.
408 (2) $HNO_3$ is generated at an input power of 100 W when the NO and $NO_x$ concentrations
409 decrease. However, $HNO_3$ is not significantly generated under the other conditions. To
410 generate $HNO_3$, reduced NO and $NO_x$ react with some active oxygen species and then
411 with vapor. The $O_3$ concentration decreases, and the $HNO_3$ concentration increases with
412 increasing load.
413 (3) At input powers of 200, 300, and 400 W, PM removal of more than 98 % and HC
414 removal of 57 % are achieved at all loads by the oxidation with the active oxygen

species such as oxygen and hydroxyl radicals. However, NO and $NO_x$ concentrations increase after treatment owing to the formation by the active nitrogen generated in the reactor.

(4) More than 98 % removal of PM, 70 % removal of $NO_x$, and 67 % removal of HC are achieved at a specific energy of 634 J/L. Because the removal of HC is almost constant, the exhaust gas contains a certain concentration of hydrocarbons which are difficult to be decomposed by the plasma.

(5) The experimental results reveal that $NO_x$, PM, and HC in diesel engine exhaust can be treated simultaneously using a surface discharge plasma reactor. Combined with a wet scrubber for $HNO_3$ removal and a catalyst bed for $O_3$ removal followed by the plasma reactor, absorption, neutralization, and removal enable the total pollution control system.

**Acknowledgments**

The authors acknowledge the cooperation of Mr. Ryotaro Tamaoki, an undergraduate student of mechanical engineering at Osaka Prefecture University, in conducting this research. This study was partially supported by JSPS KAKENHI Grant Number JP20H02374 and JP23H01626.

## References


[1] Kuwahara T, Yoshida K, Kuroki T, Hanamoto K, Sato K, Okubo M. Pilot-Scale combined reduction of accumulated particulate matter and $NO_x$ using nonthermal plasma for marine diesel engine. IEEE Trans Ind Appl 2020; 56 (2): 1804–14.

[2] Kim HJ, Kim M, Han B, Woo CG, Zouaghi A, Zouzou N, Kim YJ. Fine particle removal by a two-stage electrostatic precipitator with multiple ion-injection-type prechargers. J Aerosol Sci 2019; 130: 61–75.

[3] Kim M, Lim GT, Kim YJ, Han B, Woo CG, Kim HJ. A novel electrostatic precipitator-type small air purifier with a carbon fiber ionizer and an activated carbon fiber filter. J Aerosol Sci 2018; 117:63–73.

[4] Okubo M. Recent Development of Technology in Scale-up of Plasma Reactors for Environmental and Energy Applications, Springer, Plasma Chem Plasma Process 2022; 42: 3–33.

[5] Ni P, Wang X, Li H. A review on regulations, current status, effects and reduction strategies of emissions for marine diesel engines. Fuel 2020; 279: 118477.

[6] Xiao X, Xian C, He G, Liao C, Hu C. Current status of NOx emission treatment in marine diesel engine, Earth and Environmental Sci, IOP Conf Ser 2020; 474: 022028.

[7] Shi Y, He Y, Cai Y, Li Z, Wang W, Zhou Y, Lu Y, Yang Y. Effect of nonthermal plasma with different ozone concentrations on the oxidation and removal of different components in

453 particulate matter. J the Energy Inst 2022; 102: 268–77.

454 [8] Sonawane U, Agarwal AK. Engine emission control devices for particulate matter and

455 oxides of nitrogen: challenges and emerging trends. In: Singh, A.P., Agarwal, A.K. (eds)

456 Novel Internal Combustion Engine Technologies for Performance Improvement and

457 Emission Reduction. Energy, Environment, and Sustainability. Springer, Singapore.

458 [9] Holub M. Engine emission control: ozone and plasma desorption. Encyclopedia of

459 Plasma Technology, Edition1st Edition. CRC Press 2016; 9.

460 [10] Wongchang T, Sittichompoo S, Theinnoi K, Sawatmongkhon B, Jugjai S. Impact of

461 high-voltage discharge after-treatment technology on diesel engine particulate matter

462 composition and gaseous emissions. ACS Omega 2021; 6 (32): 21181–92.

463 [11] Zhang Z, Sui Z, Song C, Lu W, Fan X, Li H, Wang P. Research status of engine

464 emissions treated by nonthermal plasma. Environ Technol Innov 2023; 29: 103007.

465 [12] Park C, Kim C, Kim K, Lee D, Song Y, Moriyoshi Y. The influence of

466 hydrogen-enriched gas on the performance of lean NOx trap catalyst for a light-duty diesel

467 engine. Int J Hydrogen Energy 2010; 35 (4): 1789–96.

468 [13] Xia C, Zhu Y, Zhou S, Peng H, Feng Y, Zhou W, Shi J. Simulation study on transient

469 performance of a marine engine matched with high-pressure SCR system. Int J Engine Res

470 2022; 24 (4): https://doi.org/10.1177/14680874221084052

471 [14] Zhang Y, Xia C, Liu D, Zhu Y, Feng Y. Experimental investigation of the high-pressure

472 SCR reactor impact on a marine two-stroke diesel engine. Fuel 2023; 335: 127064.
473 [15] Xia C, Zhu Y, Liu D, Zhou S, Feng Y, Shi J, Yang Jun Y. Newly developed detailed
474 urea decomposition mechanism by marine engine urea-SCR system crystallization test and
475 DFT calculations. Chem Eng J 2023; 470: 144176.
476 [16] Okubo M. and Kuwahara T. New Technologies for Emission Control in Marine Diesel
477 Engines: Butterworth-Heinemann, imprint of Elsevier, 2019.
478 [17] Palma V, Ciambelli P, Meloni E, Sin A. Catalytic DPF microwave assisted active
479 regeneration. Fuel 2015; 140:50–61.
480 [18] Palma V, Ciambelli P, Meloni E, Sin A. Study of the catalyst load for a microwave
481 susceptible catalytic DPF. Catal Today 2013; 216 (6): 185–93.
482 [19] Huang Y, Ng ECY, Surawski NC, Zhou JL, Wang X, Gao J, Lin W, Brown RJ. Effect
483 of diesel particulate filter regeneration on fuel consumption and emissions performance
484 under real-driving conditions. Fuel 2022; 320: Article 123937.
485 [20] Okubo M, Arita N, Kuroki T, Yoshida K, Yamamoto T. Total diesel emission control
486 technology using ozone injection and plasma desorption. Plasma Chem Plasma Process
487 2008; 28 (2): 173–87.
488 [21] Babaie M, Davari P, Talebizadeh P, Zare F, Rahimzadeh H, Ristovski Z. Chem. Eng. J
489 2015; 276 (2): 240–48.
490 [22] Pu X, Cai Y, Shi Y, Wang J, Gu L, Tian J, Fan R. Carbon deposit incineration during

engine flameout using non-thermal plasma injection. Int J Automot Technol 2018; 19: 421–32.

[23] Ranji-Burachaloo H, Masoomi-Godarzi S, Khodadadi AA, Mortazavi Y. Synergetic effects of plasma and metal oxide catalysts on diesel soot oxidation. Appl Catal B 2016; 182: 74–84.

[24] Ji L, Cai Y, Shi Y, Fan R, Wang W, Chen Y. Effects of nonthermal plasma on microstructure and oxidation characteristics of particulate matter. Environ Sci Technol 2020; 54: 2510–19.

[25] Kuwahara T, Yoshida K, Hanamoto K, Sato K, Kuroki T, Okubo M. Effect of exhaust gas temperature on oxidation of marine diesel emission particulates with nonthermal-plasma-induced ozone. Ozone Sci Eng 2015; 37 (6): 518–26.

[26] Yao S, Kodama S, Yamamoto S, Fushimi C. Characterization of an uneven DBD reactor for diesel PM removal. Asia-Pac J Chem Eng 2009; 5 (5): 701–7.

[27] Okubo M, Kuroki T, Yoshida K, Yamamoto T. Single-stage simultaneous reduction of diesel particulate and using oxygen-lean nonthermal plasma application. IEEE Trans Ind Appl 2010; 46 (6): 2143–50.

[28] Okubo M, Yamada H, Yoshida K, Kuroki T. Simultaneous reduction of diesel particulate and $NO_x$ using a catalysis-combined nonthermal plasma reactor. IEEE Trans Ind Appl 2017; 53 (6): 5875–82.

510 [29] Kuwahara T, Yoshida K, Kuroki T, Hanamoto K, Sato K, Okubo M. A pilot-scale
511 experiment for total marine diesel emission control using ozone injection and nonthermal
512 plasma reduction. IEEE Trans Ind Appl 2015; 51 (2): 1168–78.
513 [30] Shi Y, Cai Y, Li X. Wang W. Evolution of diesel particulate physicochemical properties
514 using nonthermal plasma. Fuel 2019; 253:1292–99.
515 [31] Yoshida K. Aftertreatment of carbon particles emitted by diesel engine using a
516 combination of corona and dielectric barrier discharge. IEEE Trans Ind Appl 2019; 55 (5):
517 5261–68.
518 [32] Kuwahara T, Nishii S, Kuroki T, Okubo M. Complete regeneration characteristics of
519 diesel particulate filter using ozone injection. Appl Energy 2013; 111: 652–6.
520 [33] Lin H, Huang Z, Shangguan W, Peng X. Temperature-programmed oxidation of diesel
521 particulate matter in a hybrid catalysis-plasma reactor. Proc Combust Inst 2007; 31: 3335–42.
522 [34] Babaie M, Davari P, Zare F, Rahman M, Rahimzadeh H, Ristovski Z, Brown R. Effect
523 of pulsed power on particle matter in diesel engine exhaust using a DBD plasma reactor.
524 IEEE Trans Plasma Sci 2013; 41: 2349–58.
525 [35] Babaie M, Kishi T, Arai M, Zama Y, Furuhata T, Ristovski Z, Rahimzadeh H, Brown R.
526 Influence of non-thermal plasma after-treatment technology on diesel engine particulate
527 matter composition and $NO_x$ concentration. Int J Plasma Environ Sci Technol 2016; 13:
528 221–30.

529 [36] Shi Y, Cai Y, Fan R, Cui Y, Chen Y, Ji L. Characterization of soot inside a diesel
530 particulate filter during a nonthermal plasma promoted regeneration step. Appl Therm Eng
531 2019; 150: 612–19.
532 [37] Wang P, Gu W, Lei L, Cai Y, Li Z. Micro-structural and components evolution
533 mechanism of particular matter from diesel engines with non-thermal plasma technology.
534 Appl Therm Eng 2015; 91: 1–10.
535 [38] Fan R, Cai Y, Shi Y, Cui Y. Effect of the reaction temperature on the removal of diesel
536 particulate matter by ozone injection. Plasma Chem Plasma Process 2019; 39: 143–63.
537 [39] Gu L, Cai Y, Shi Y, Wang J, Pu X, Tian J, Fan R. Effect of indirect non-thermal plasma
538 on particle size distribution and composition of diesel engine particles. Plasma Sci Technol
539 2017; 19 (11): 115503.
540 [40] Gao J, Ma C, Xing S, Sun L. Oxidation behaviours of particulate matter emitted by a
541 diesel engine equipped with a NTP device. Appl Therm Eng 2017; 119 (5): 593–602.
542 [41] Yao S, Shen X, Zhang X, Han J, Wu Z, Tang X, Lu H, Jiang B. Sustainable removal of
543 particulate matter from diesel engine exhaust at low temperature using a plasma-catalytic
544 method. Chem. Eng. J 2017; 327: 343–50.
545 [42] Naito K, Taniguchi M, Madokoro K, Shimamura R, Nadanami N, Sakai S, Takagi K,
546 Itoh S. Development of PM aftertreatment system using nonthermal plasma. Int J Automot
547 Eng 2018; 49 (2): 265–70 (in Japanese).

548 [43] Madhukar A, Rajanikanth BS. Plasma/adsorbent system for NOx treatment in diesel
549 exhaust: a case study on solid industrial wastes. Int J Environ Sci Te 2019; 16 (7):2973–88.
550 [44] Madhukar A, Rajanikanth BS. Waste foundry sand/Bauxite residue for enhanced NOx
551 reduction in diesel exhaust pre-treated with plasma/O3 injection. IEEE Trans Plasma Sci
552 2019; 47 (1): 376–86.
553 [45] Madhukar A, Rajanikanth BS. Cascaded plasma-ozone injection system: a novel
554 approach for mitigating total hydrocarbons in diesel exhaust. Plasma Chem Plasma P 2019;
555 39 (4): 845–62.
556 [46] Yamasaki H, Shidara A, Shimizu Y, Kuroki T, Kim HJ, Okubo M. In-flight diesel
557 particulate matter removal using nonthermal plasma filtering. Int J Plasma Environ Sci
558 Technol 2020; 14 (3): e03007 (total 13 pages).
559 [47] Takehana K, Kuroki T, Okubo M. Evaluation on nitrogen oxides and nanoparticle
560 removal and nitrogen monoxide generation using a wet-type nonthermal plasma reactor. J
561 Phys D: Appl Phys 2018; 51 (20): 204002.
562 [48] Kittelson, DB. Engines and nanoparticles: a review. J Aerosol Sci 1998; 29(5–6):
563 575–88.
564 [49] Zhu J, Lee KO, Yozgatligil A, Choi MY. Effects of engine operating conditions on
565 morphology, microstructure, and fractal geometry of light-duty diesel engine particulates. P
566 Combust Inst 2005; 30 (2): 2781–89.

567 [50] An P, Sun W, Li G, Tan M, Lai C, Chen S. Characteristics of particle size distributions
568 about emissions in a common-rail diesel engine with biodiesel blends. Procedia
569 Environmental Sciences 2011; 11: 1371–78.
570

571 **Figure and table captions**

572

573 **Fig. 1.** Experimental setup for diesel exhaust treatment system using a surface discharge
574 plasma reactor. (a) Schematic of experimental equipment. (b) Photograph of the diesel engine,
575 exhaust piping, apparatus, and flow directions used in the experiment.

576 **Fig. 2.** Surface discharge plasma reactor. (a) Surface discharge element and cross section of
577 the inner wall of the element. (b) Front view of the surface discharge element and the
578 high-frequency and high-voltage power supply. (c) Photograph inside the surface discharge
579 plasma reactor when the power is turned off. (d) Photograph inside the surface discharge
580 plasma reactor when the reactor input power is 400 W.

581 **Table 1.** Engine specifications and experimental conditions.

582 **Fig. 3.** Relationship between each composition of the raw exhaust gas components and the
583 engine load.

584 **Fig. 4.** Particle concentration before and after plasma treatment for engine loads of: (a) 0 %,
585 (b) 25 %, (c) 50 %, and (d) 75 %. The white symbol indicates particle concentration before
586 treatment, and the colored symbols indicate the particle concentration after treatment with
587 input power of 100, 200, 300, and 400 W. Each symbol and error bar represent the average
588 value of the measurements and the standard deviation $\pm\sigma$, respectively.

589 **Fig. 5.** Particle removal efficiency for engine loads of: (a) 0 %, (b) 25 %, (c) 50 %, and (d)

590 75 %. Symbols indicate the average removal efficiency after treatment with input power of

591 100, 200, 300, and 400 W.

592 **Fig. 6.** Time-dependent gaseous concentrations (input power *P* = 100 W) for various engine

593 loads of: (a) 0 %, (b) 25 %, (c) 50 %, and (d) 75 %.

594 **Fig. 7.** Typical time-dependent gaseous concentrations (engine load = 75 %; input power =

595 400 W).

596 **Fig. 8.** Gaseous concentrations before and after treatment for various engine load, with an

597 input power of: (a) 100 W, (b) 200 W, (c) 300 W, and (d) 400 W. The solid lines indicate the

598 gaseous concentrations after treatment, and the dotted lines indicate the gaseous

599 concentrations before treatment.

600 **Fig. 9.** $NO_x$, PM, and HC removal efficiencies for various specific energy. Symbols indicate

601 the removal efficiencies of $NO_x$, PM, and HC, respectively.

602

603

## Figures and Table

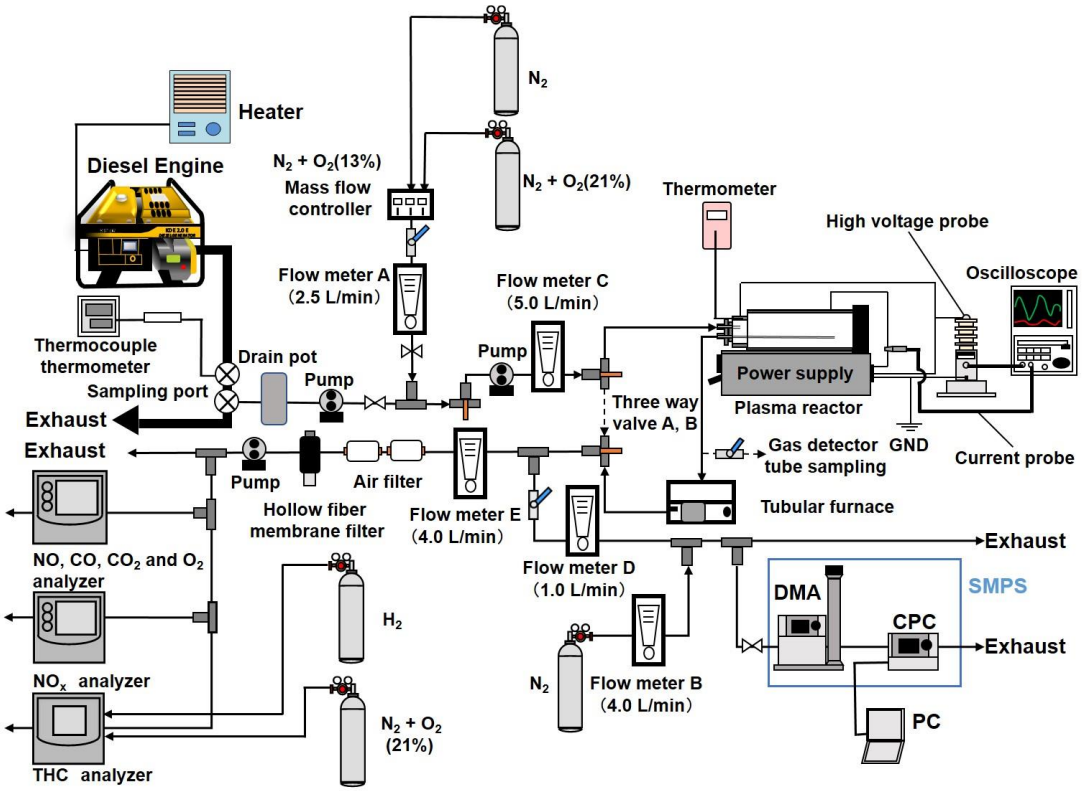


(a)

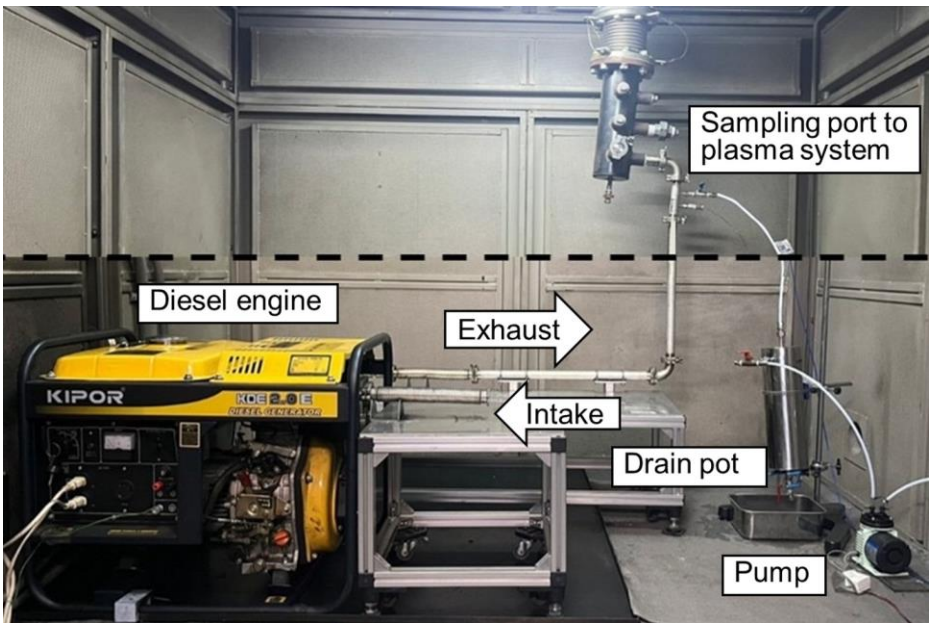


(b)

**Fig. 1.**

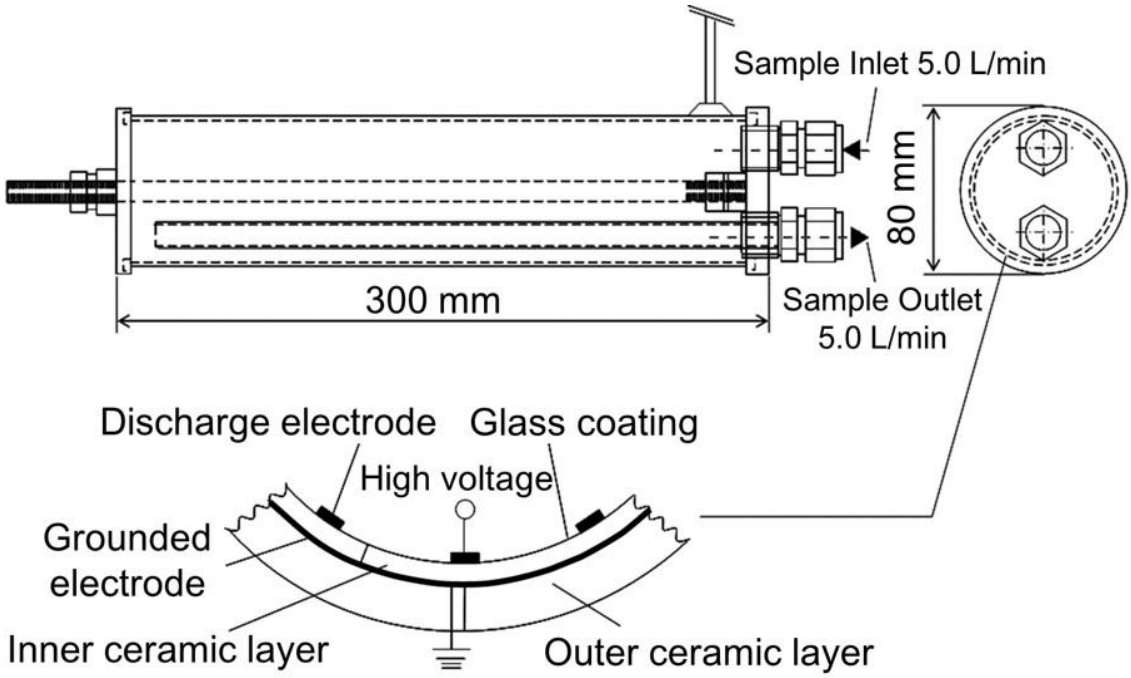
Sample Inlet 5.0 L/min
80 mm
300 mm
Sample Outlet
5.0 L/min
Discharge electrode
Glass coating
High voltage
Grounded
electrode
Inner ceramic layer
Outer ceramic layer

(a)

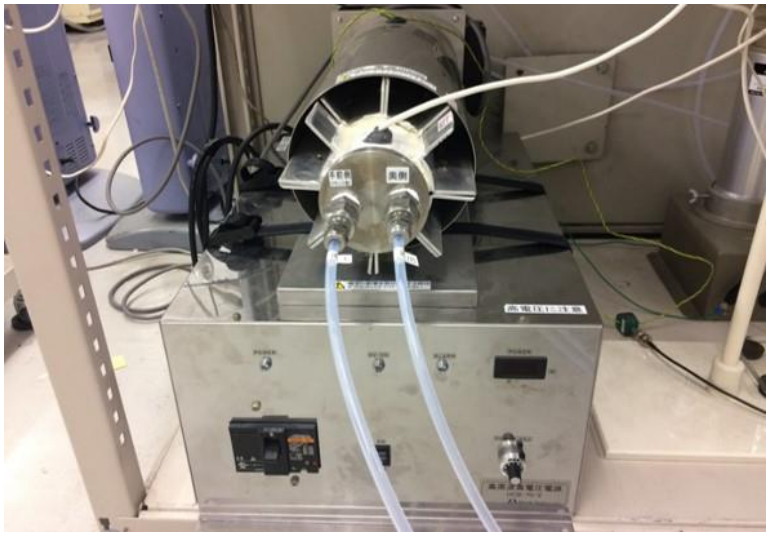

(b)

**Fig. 2.**

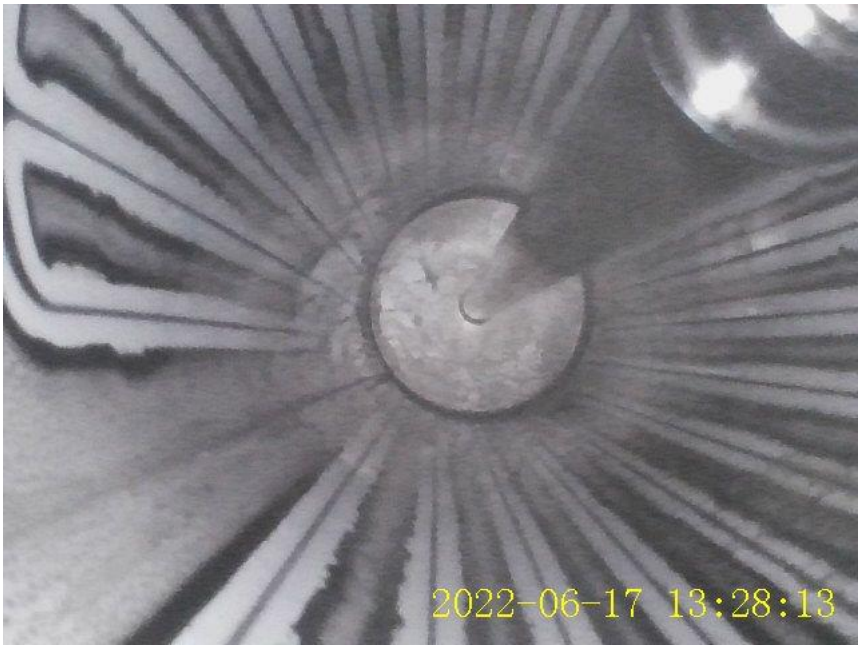


(c)

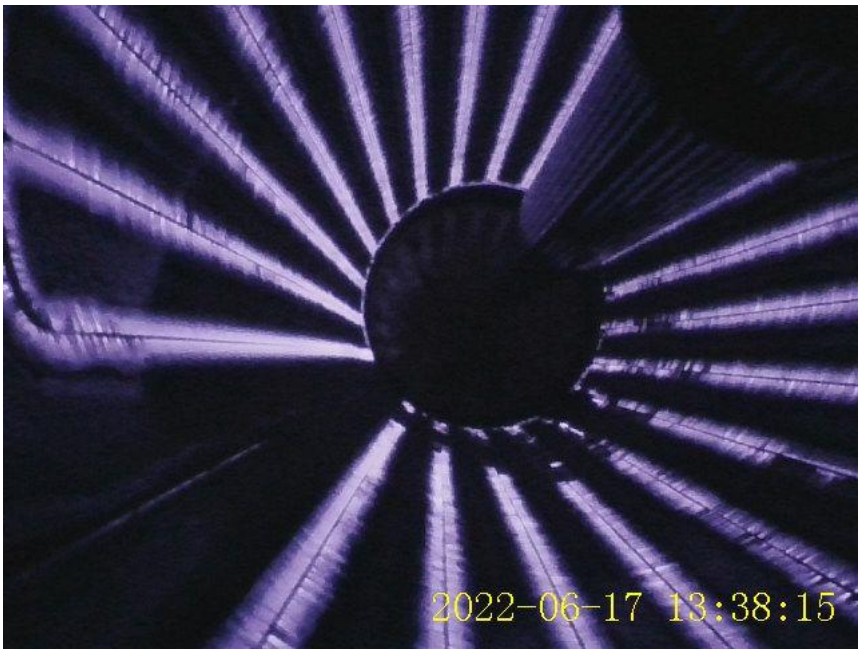


(d)

**Fig. 2.**

**Table 1.**

| Load, % | 0 | 25 | 50 | 75 |
|---|---|---|---|---|
| Number of cylinder | 1 | | | |
| Diameter of cylinder, mm | 70 | | | |
| Stroke of cylinder, mm | 55 | | | |
| Displacement volume, mL | 211 | | | |
| Rotating speed, rpm | 3600 | | | |
| Power, kW | 0 | 0.5 | 1.0 | 1.5 |
| Dry weight of engine, kg | 60 | | | |

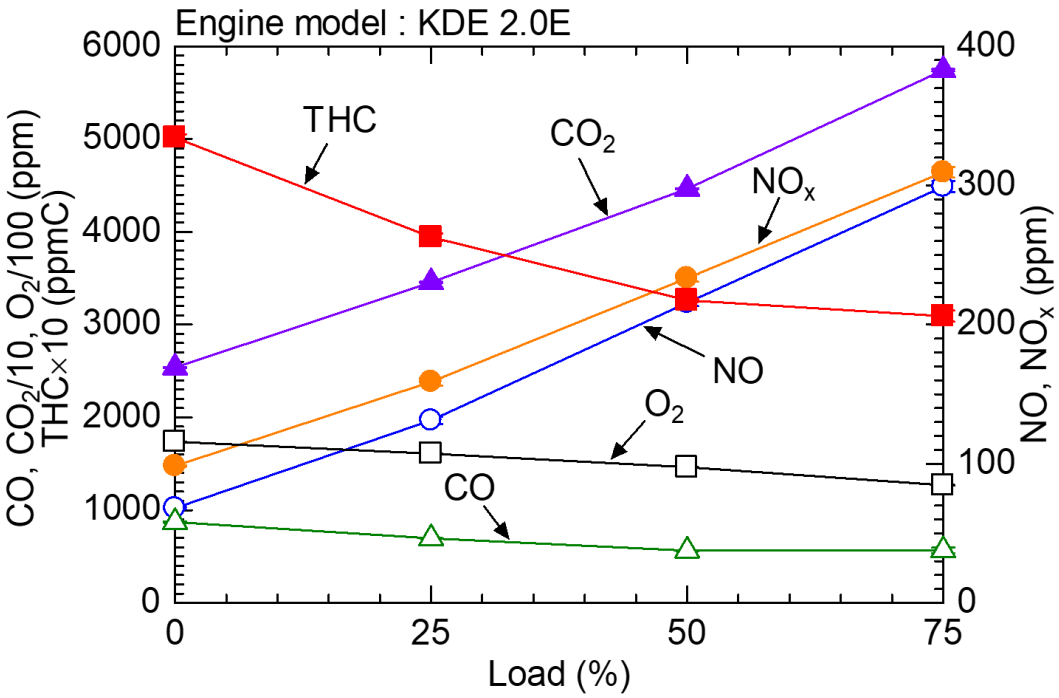
Engine model : KDE 2.0E
THC
CO2
NOx
NO
O2
CO
CO, CO2/10, O2/100 (ppm)
THC×10 (ppmC)
NO, NOx (ppm)
Load (%)
6000
5000
4000
3000
2000
1000
0
400
300
200
100
0
0
25
50
75

**Fig. 3.**

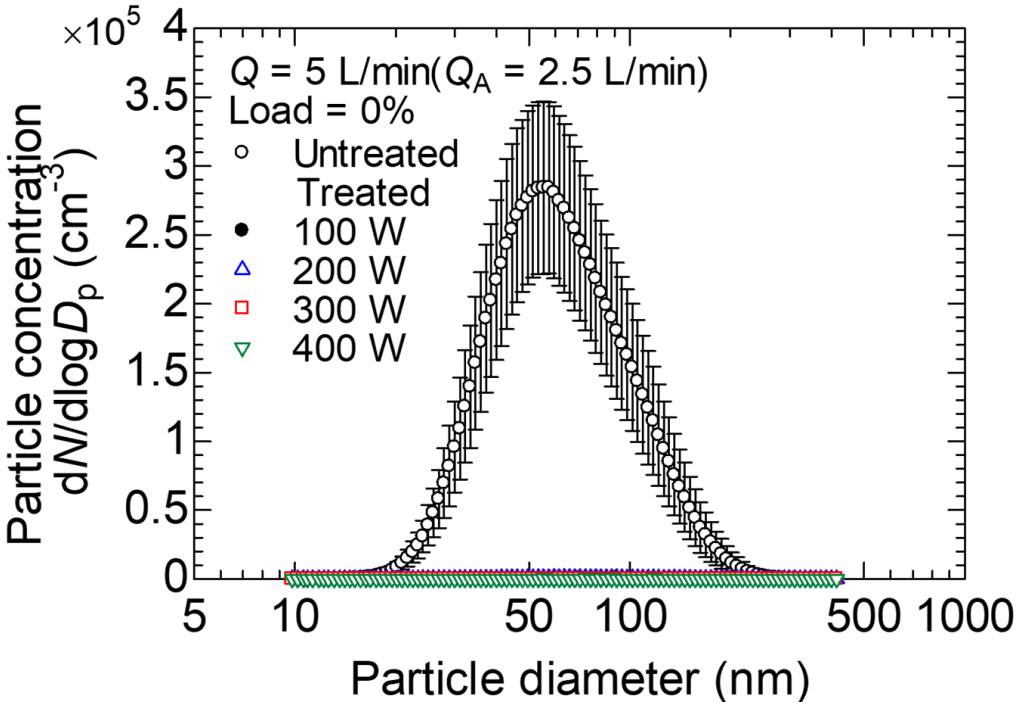
×10^5
Q = 5 L/min(Q_A = 2.5 L/min)
Load = 0%
Untreated
Treated
100 W
200 W
300 W
400 W
Particle concentration
dN/dlogD_p (cm^-3)
Particle diameter (nm)

(a)

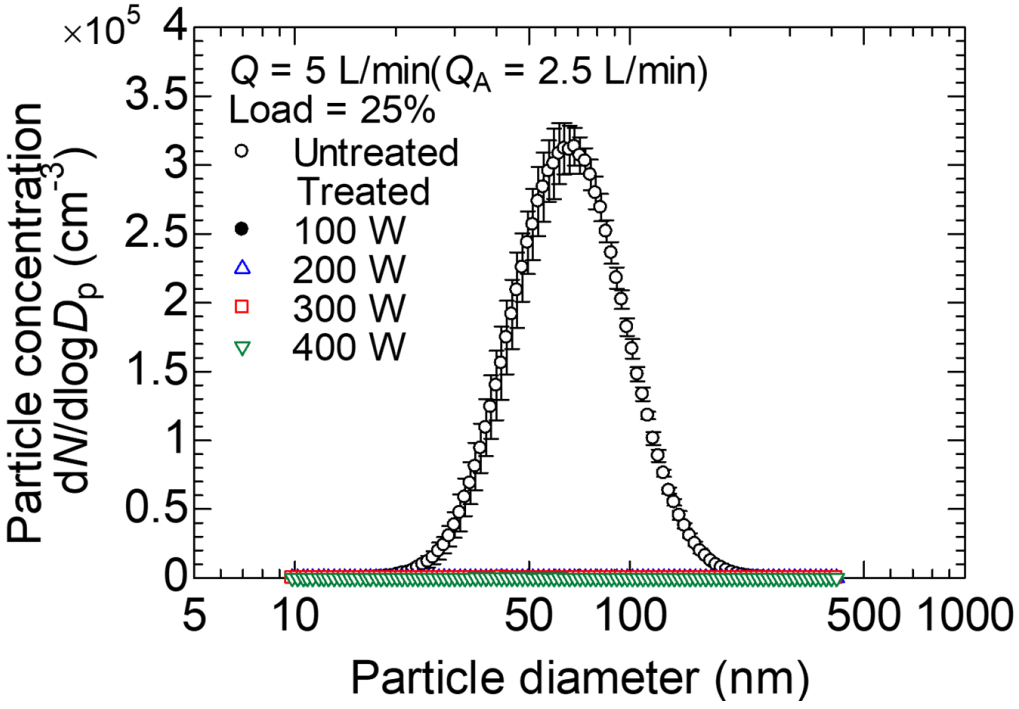
×10^5
Q = 5 L/min(Q_A = 2.5 L/min)
Load = 25%
Untreated
Treated
100 W
200 W
300 W
400 W
Particle concentration
dN/dlogD_p (cm^-3)
Particle diameter (nm)

(b)

**Fig. 4.**

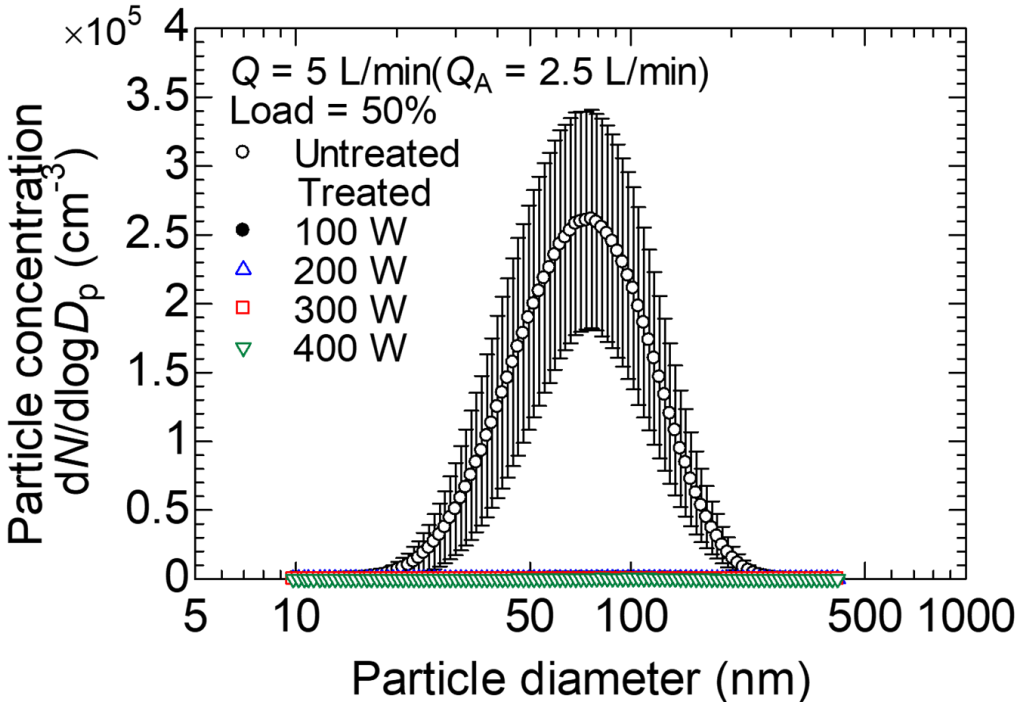
×10^5
Q = 5 L/min(Q_A = 2.5 L/min)
Load = 50%
Untreated
Treated
100 W
200 W
300 W
400 W
Particle concentration dN/dlogD_p (cm^-3)
Particle diameter (nm)

(c)

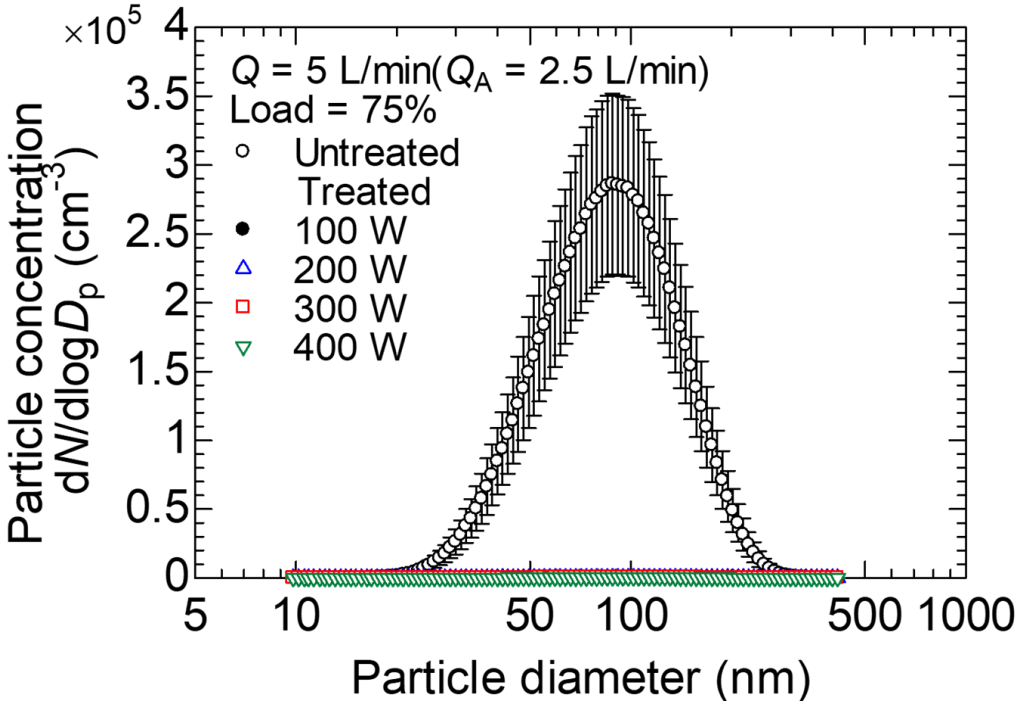
×10^5
Q = 5 L/min(Q_A = 2.5 L/min)
Load = 75%
Untreated
Treated
100 W
200 W
300 W
400 W
Particle concentration dN/dlogD_p (cm^-3)
Particle diameter (nm)

(d)

**Fig. 4.**

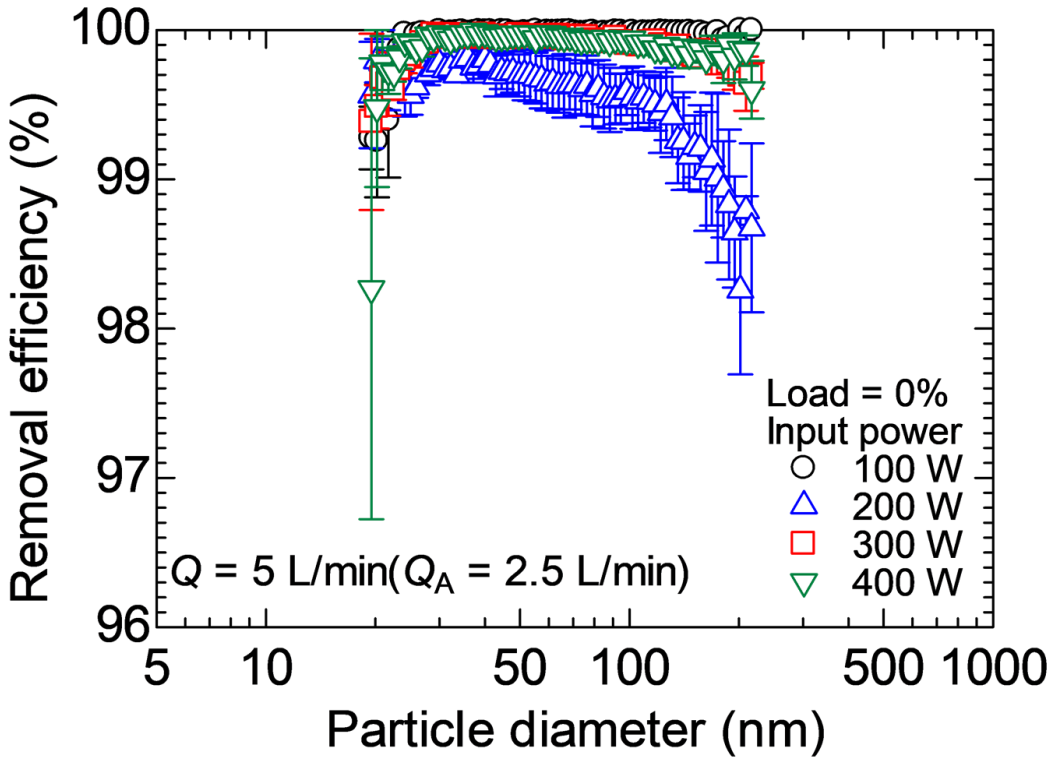
Removal efficiency (%)
100
99
98
97
96
5
10
50
100
500
1000
Particle diameter (nm)
Q = 5 L/min(Q_A = 2.5 L/min)
Load = 0%
Input power
100 W
200 W
300 W
400 W

(a)

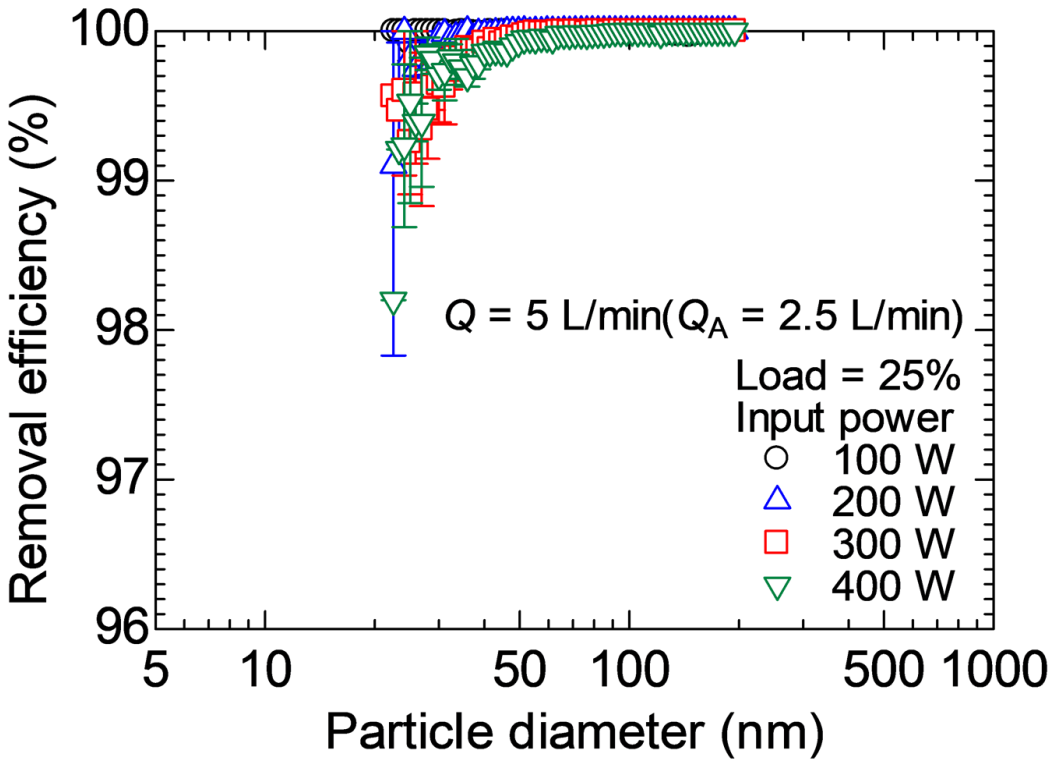
Removal efficiency (%)
100
99
98
97
96
5
10
50
100
500
1000
Particle diameter (nm)
Q = 5 L/min(Q_A = 2.5 L/min)
Load = 25%
Input power
100 W
200 W
300 W
400 W

(b)

**Fig. 5.**

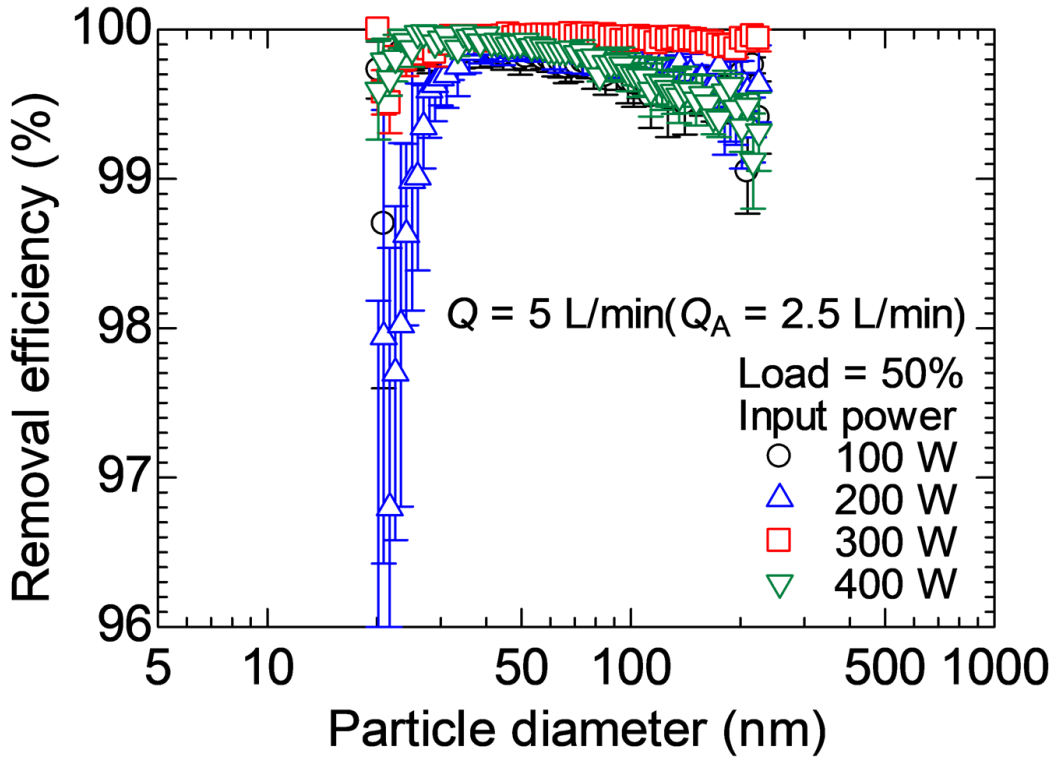
Removal efficiency (%)
100
99
98
97
96
5
10
50
100
500
1000
Particle diameter (nm)
Q = 5 L/min(Q_A = 2.5 L/min)
Load = 50%
Input power
100 W
200 W
300 W
400 W

(c)

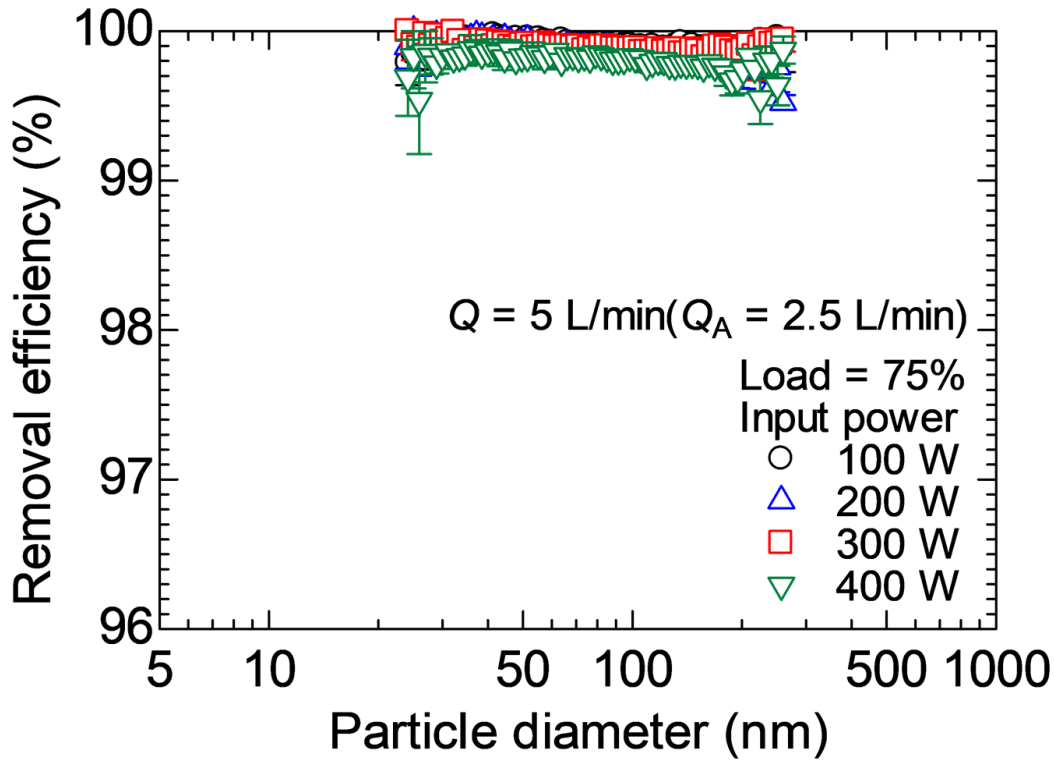
Removal efficiency (%)
100
99
98
97
96
5
10
50
100
500
1000
Particle diameter (nm)
Q = 5 L/min(Q_A = 2.5 L/min)
Load = 75%
Input power
100 W
200 W
300 W
400 W

(d)

**Fig. 5.**

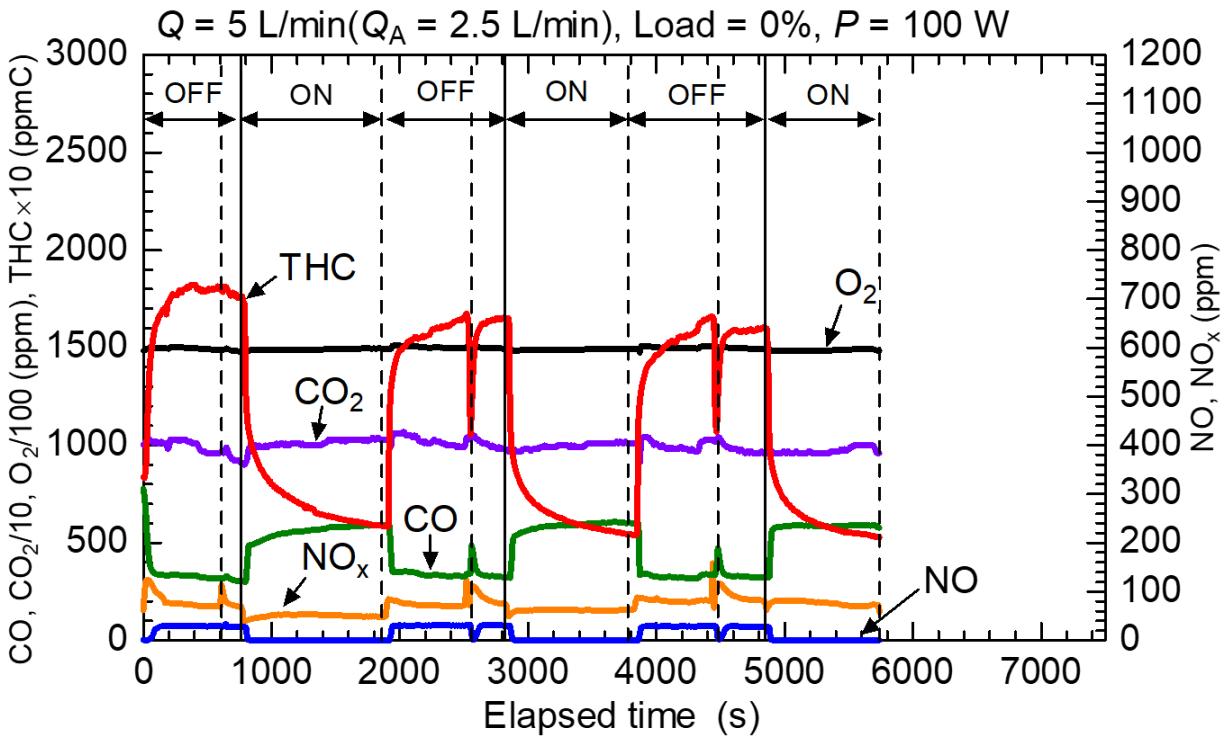
Q = 5 L/min(Q_A = 2.5 L/min), Load = 0%, P = 100 W
OFF
ON
OFF
ON
OFF
ON
THC
O2
CO2
CO
NOx
NO
CO, CO2/10, O2/100 (ppm), THC×10 (ppmC)
NO, NOx (ppm)
Elapsed time (s)

(a)

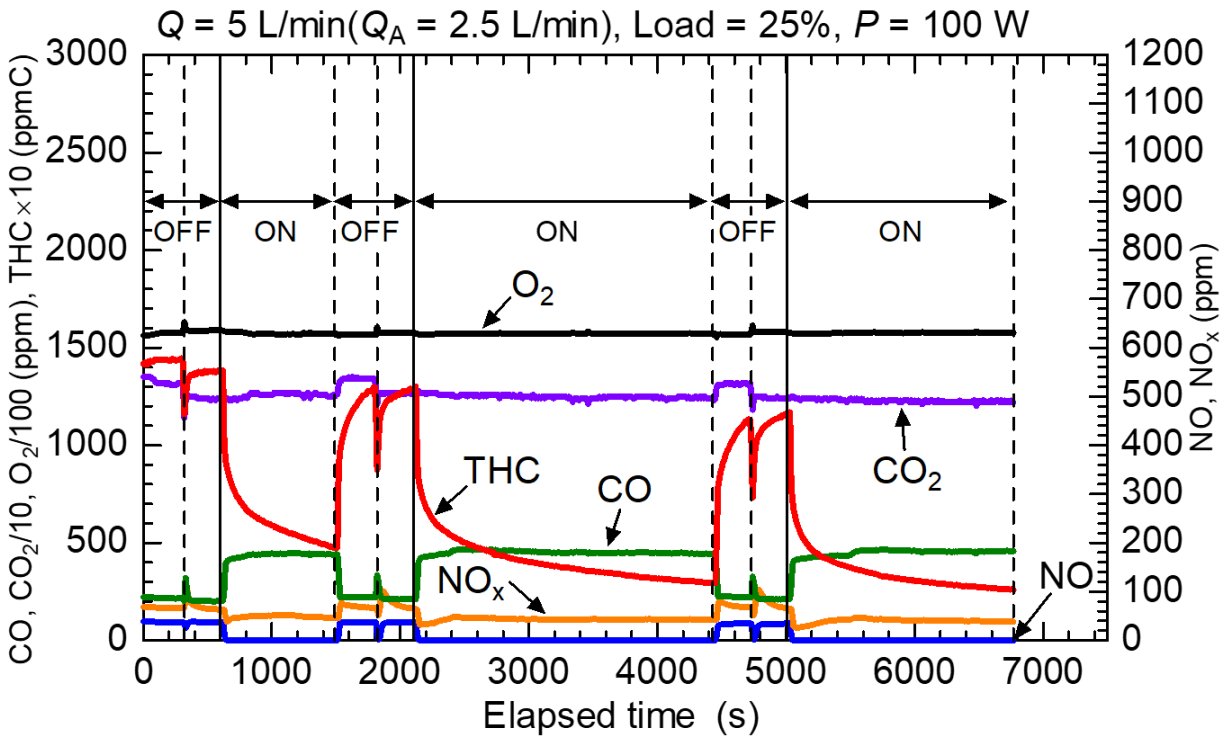
Q = 5 L/min(Q_A = 2.5 L/min), Load = 25%, P = 100 W
OFF
ON
OFF
ON
OFF
ON
O2
THC
CO
CO2
NOx
NO
CO, CO2/10, O2/100 (ppm), THC×10 (ppmC)
NO, NOx (ppm)
Elapsed time (s)

(b)

**Fig. 6.**

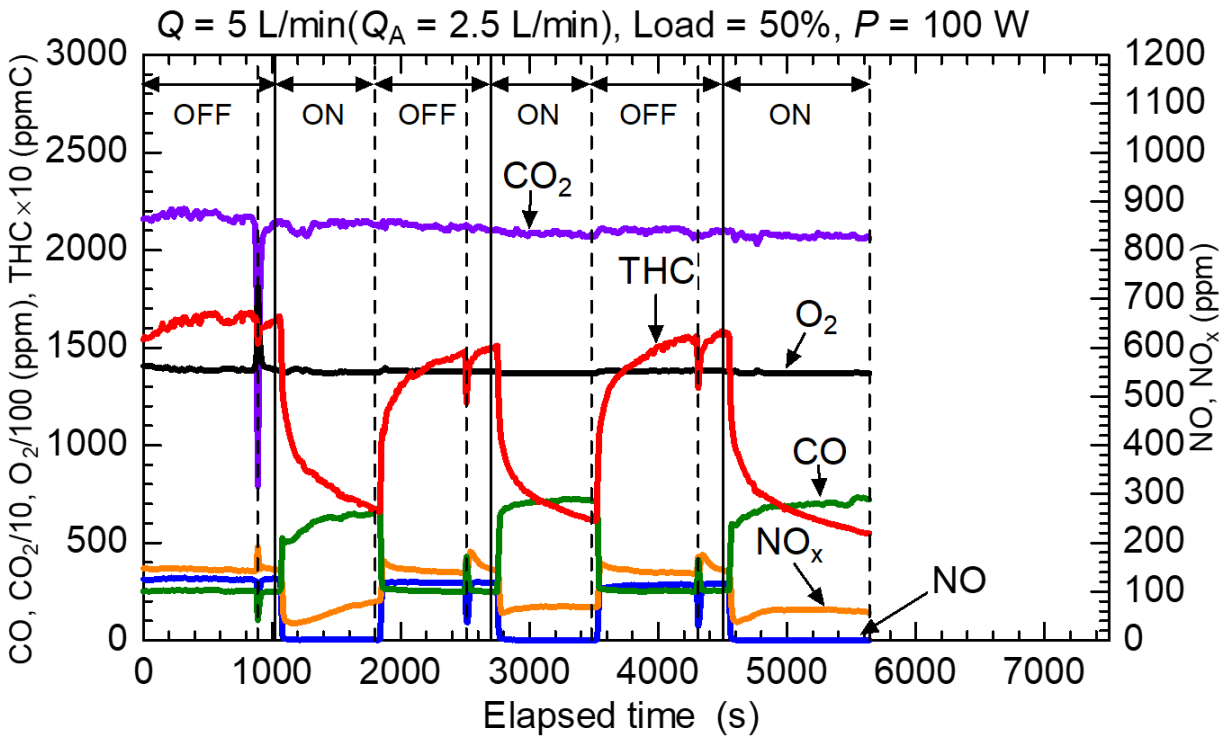
Q = 5 L/min(Q_A = 2.5 L/min), Load = 50%, P = 100 W
OFF
ON
OFF
ON
OFF
ON
CO2
THC
O2
CO
NOx
NO
CO, CO2/10, O2/100 (ppm), THC×10 (ppmC)
NO, NOx (ppm)
Elapsed time (s)

(c)

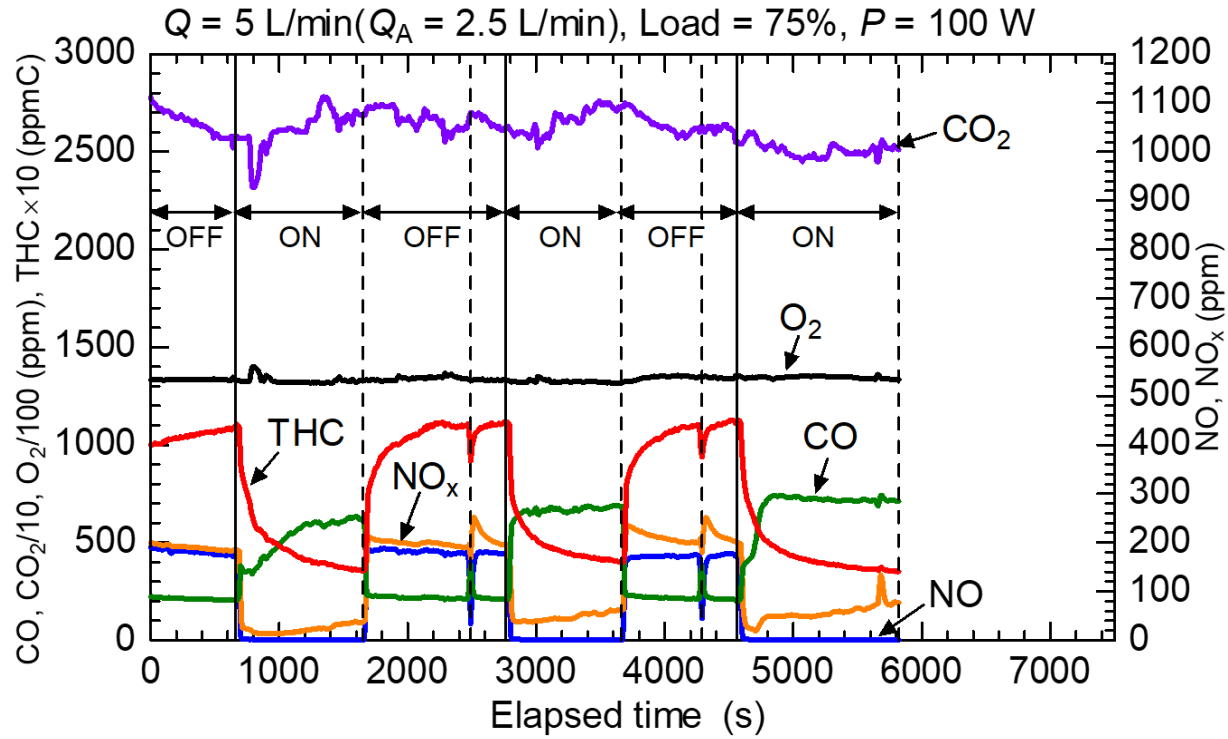
Q = 5 L/min(Q_A = 2.5 L/min), Load = 75%, P = 100 W
OFF
ON
OFF
ON
OFF
ON
CO2
O2
THC
NOx
CO
NO
CO, CO2/10, O2/100 (ppm), THC×10 (ppmC)
NO, NOx (ppm)
Elapsed time (s)

(d)

**Fig. 6.**

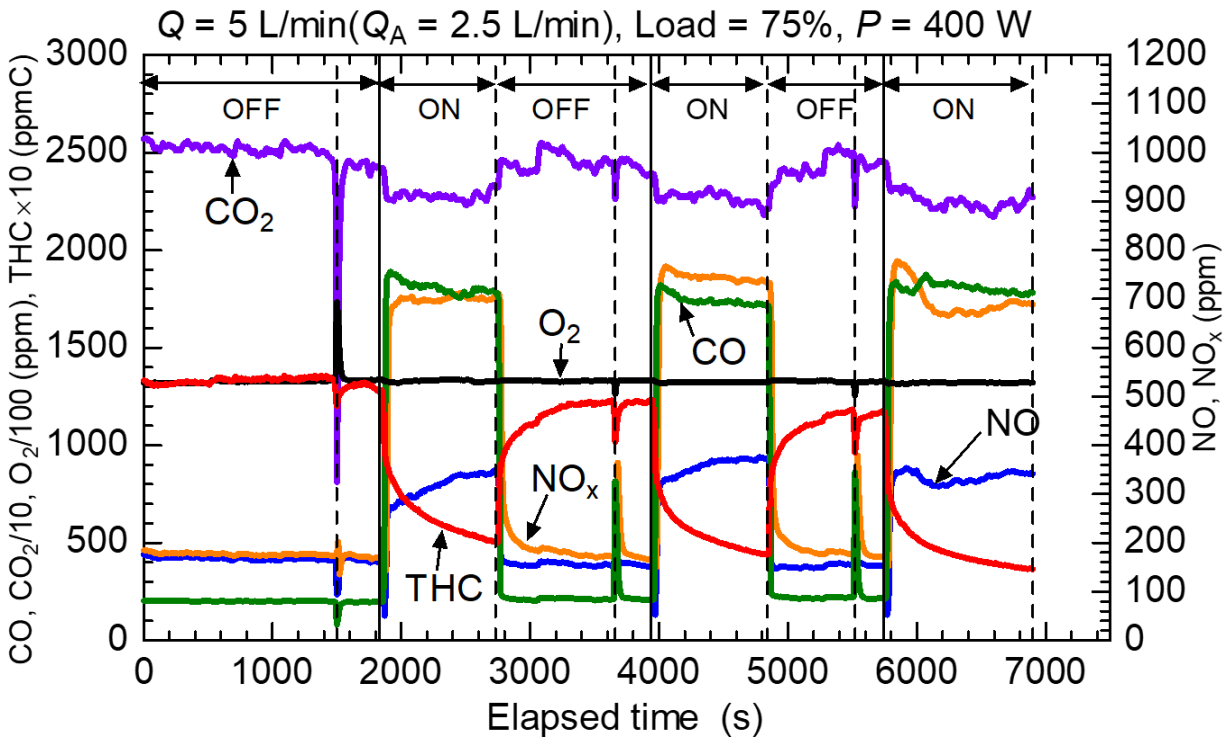
Q = 5 L/min(Q_A = 2.5 L/min), Load = 75%, P = 400 W
OFF
ON
OFF
ON
OFF
ON
CO2
O2
CO
NOx
NO
THC
CO, CO2/10, O2/100 (ppm), THC×10 (ppmC)
NO, NOx (ppm)
Elapsed time (s)
0
500
1000
1500
2000
2500
3000
0
100
200
300
400
500
600
700
800
900
1000
1100
1200
0
1000
2000
3000
4000
5000
6000
7000

**Fig. 7.**

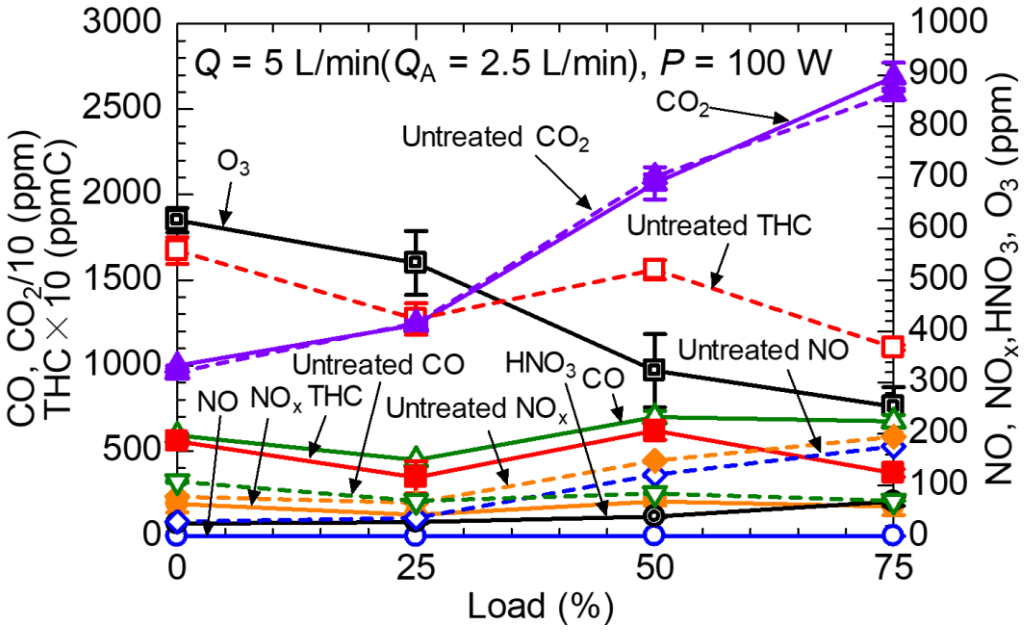
Q = 5 L/min(Q_A = 2.5 L/min), P = 100 W
CO, CO2/10 (ppm)
THC×10 (ppmC)
NO, NOx,HNO3, O3 (ppm)
Load (%)
O3
CO2
Untreated CO2
Untreated THC
Untreated NO
Untreated CO
HNO3
CO
NO
NOx
THC
Untreated NOx

(a)

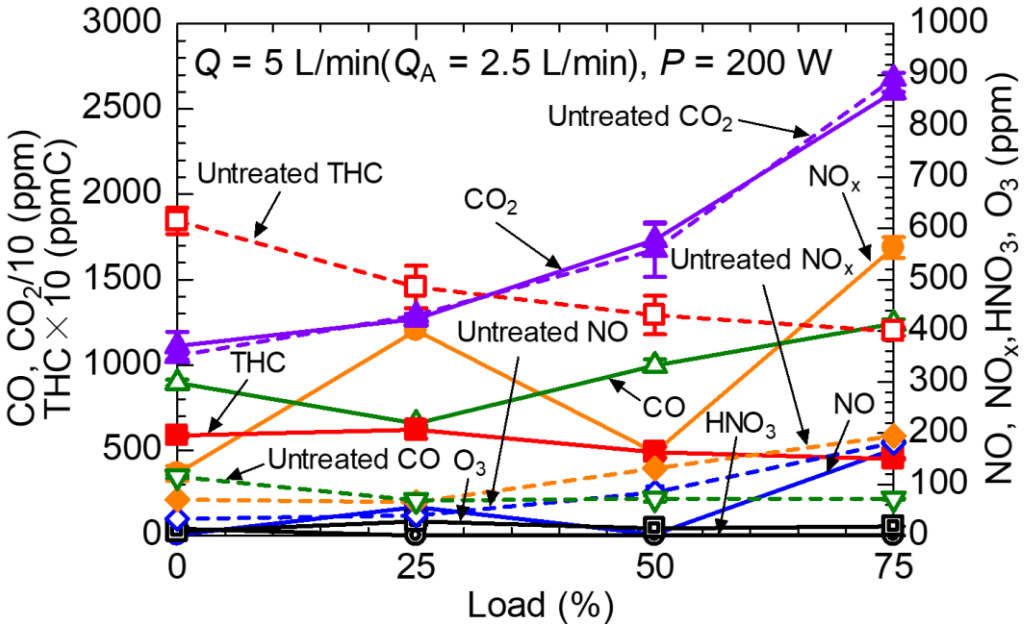
Q = 5 L/min(Q_A = 2.5 L/min), P = 200 W
CO, CO2/10 (ppm)
THC×10 (ppmC)
NO, NOx,HNO3, O3 (ppm)
Load (%)
Untreated CO2
Untreated THC
CO2
NOx
Untreated NOx
Untreated NO
THC
CO
HNO3
NO
Untreated CO
O3

(b)

**Fig. 8.**

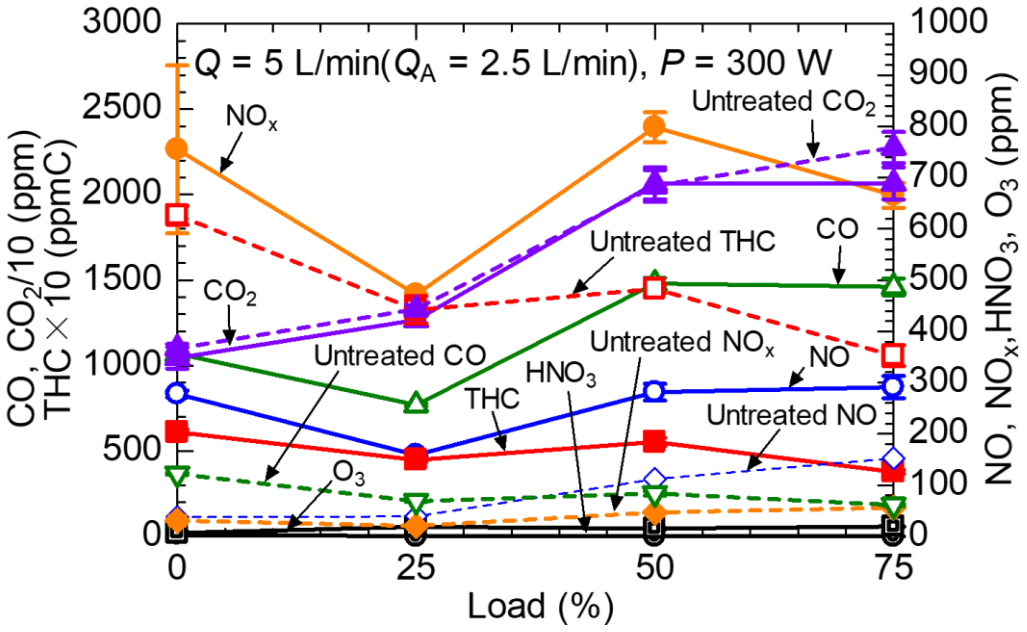
Q = 5 L/min(Q_A = 2.5 L/min), P = 300 W
NO_x
Untreated CO_2
Untreated THC
CO
CO_2
Untreated CO
Untreated NO_x
NO
HNO_3
THC
Untreated NO
O_3
CO, CO_2/10 (ppm)
THC×10 (ppmC)
NO, NO_x,HNO_3, O_3 (ppm)
Load (%)

(c)

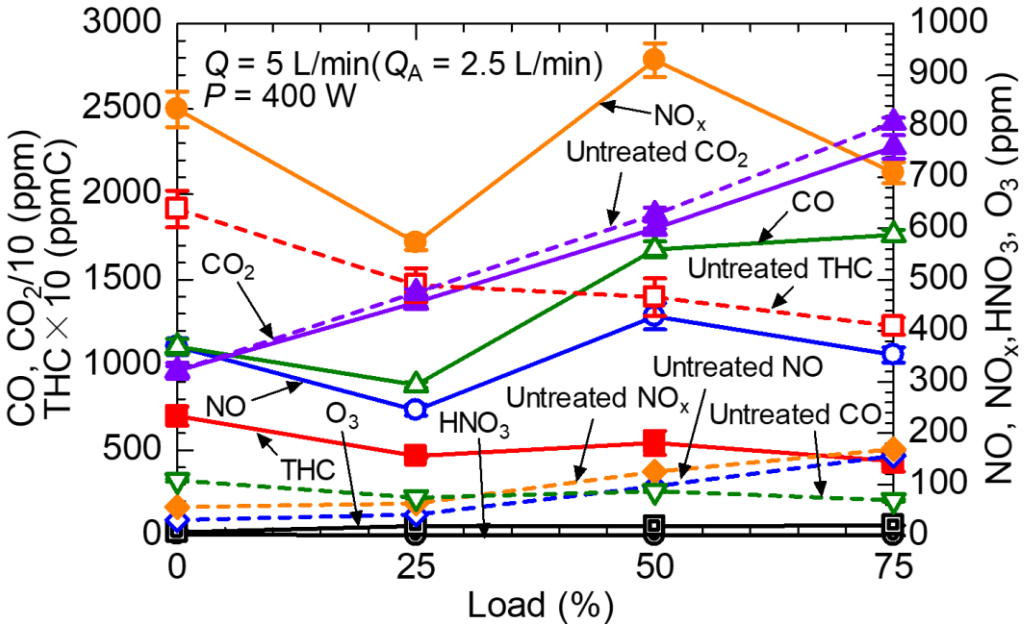
Q = 5 L/min(Q_A = 2.5 L/min)
P = 400 W
NO_x
Untreated CO_2
CO
CO_2
Untreated THC
Untreated NO
NO
O_3
HNO_3
Untreated NO_x
Untreated CO
THC
CO, CO_2/10 (ppm)
THC×10 (ppmC)
NO, NO_x,HNO_3, O_3 (ppm)
Load (%)

(d)

**Fig. 8.**

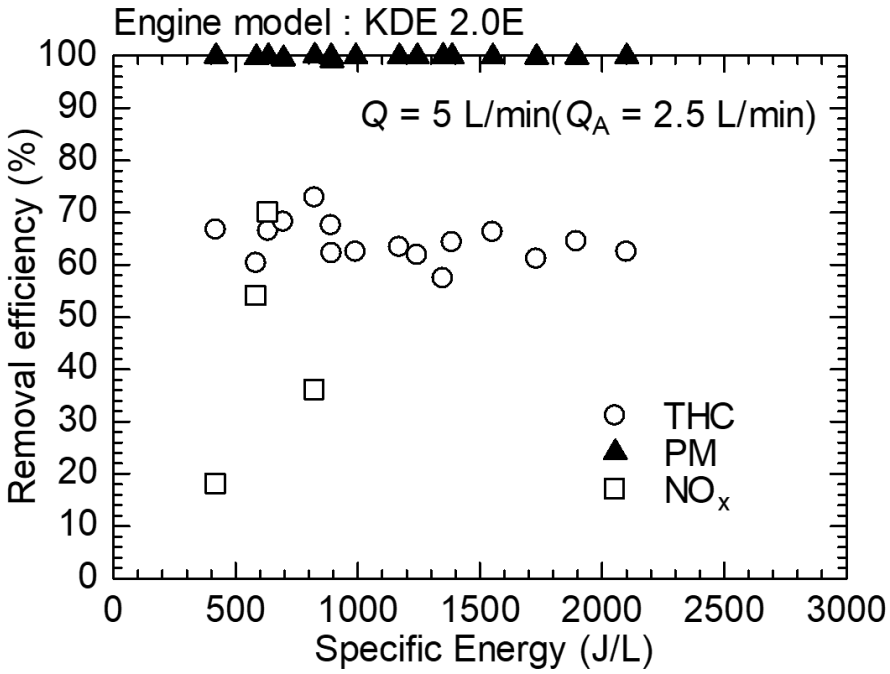
Engine model : KDE 2.0E
Q = 5 L/min(Q_A = 2.5 L/min)
THC
PM
NO_x
Removal efficiency (%)
Specific Energy (J/L)
0
10
20
30
40
50
60
70
80
90
100
0
500
1000
1500
2000
2500
3000

**Fig. 9.**